Science of the Total Environment 838 (2022) 155660

Contents lists available at ScienceDirect

Science of the Total Environment

journal homepage: www.elsevier.com/locate/scitotenv

Fires, vegetation, and human—The history of critical transitions during the last 1000 years in Northeastern Mongolia

Michał Słowiński [a,*,1], Milena Obremska [b,1], Dashtseren Avirmed [c], Michał Woszczyk [d], Saruulzaya Adiya [c], Dominika Łuców [a], Agnieszka Mroczkowska [a,i], Agnieszka Halaś [a], Witold Szczuciński [e], Andrzej Kruk [f], Mariusz Lamentowicz [g], Joanna Stańczak [b], Natalia Rudaya [h]

[a] Past Landscape Dynamics Laboratory, Institute of Geography and Spatial Organisation, Polish Academy of Sciences, Warsaw, Poland
[b] Institute of Geological Sciences, Polish Academy of Sciences, Warsaw, Poland
[c] Institute of Geography and Geoecology, Mongolian Academy of Sciences, Ulaanbaatar, Mongolia
[d] Biogeochemistry Research Unit, Adam Mickiewicz University, Poznań, Poland
[e] Geohazards Research Unit, Institute of Geology, Adam Mickiewicz University, Poznań, Poland
[f] Department of Ecology and Vertebrate Zoology, Faculty of Biology and Environmental Protection, University of Lodz, Łódź, Poland
[g] Climate Change Ecology Research Unit, Adam Mickiewicz University, Poznań, Poland
[h] PaleoData Lab, Institute of Archaeology and Ethnography SB RAS, Novosibirsk, Russia
[i] Department of Geology and Geomorphology, Faculty of Geographical Sciences, University of Lodz, Lodz, Poland

HIGHLIGHTS

- New peat record from the permafrost marginal zone of Central Asia (Mongolia)
- The first high-resolution fire history from Northern Mongolia covering the last 1000 years
- Deadly combination of droughts and snowy winters called “dzud” affect fire intensity.
- The ecosystems of Central Mongolia are sensitive to a rapidly changing climate.
- Climate, permafrost, and vegetation changes affect the nomadic societies in Mongolia.

GRAPHICAL ABSTRACT

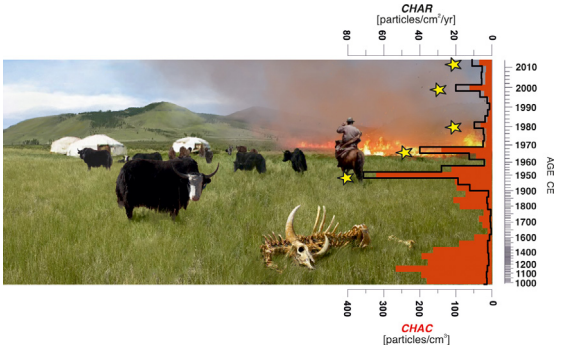

ARTICLE INFO

Editor: Elena Paoletti

Keywords:
Pollen
Charcoal
Geochemistry
Dzud
Climate change
Khentii Mountains
Central Asia

ABSTRACT

Fires are natural phenomena that impact human behaviors, vegetation, and landscape functions. However, the long-term history of fire, especially in the permafrost marginal zone of Central Asia (Mongolia), is poorly understood. This paper presents the results of radiocarbon and short-lived radionuclides (^{210}Pb and ^{137}Cs) dating, pollen, geochemical, charcoal, and statistical analyses (Kohonen's artificial neural network) of sediment core obtained from Northern Mongolia (the Khentii Mountains region). Therefore, we present the first high-resolution fire history from Northern Mongolia covering the last 1000 years, based on a multiproxy analysis of peat archive data. The results revealed that most of the fires in the region were likely initiated by natural factors, which were probably related to heatwaves causing prolonged droughts. We have demonstrated the link between enhanced fires and “dzud”, a local climatic phenomenon. The number of livestock, which has been increasing for several decades, and the observed climatic changes are superimposed to cause “dzud”, a deadly combination of droughts and snowy winter, which affects fire intensity. We observed that the study area has a sensitive ecosystem that reacts quickly to climate change. In terms of changes in the vegetation, the reconstruction reflected climate variations during the last millennium, the degradation of

* Corresponding author.
E-mail address: michal.slowinski@geopan.torun.pl (M. Słowiński).
[1] These authors contributed equally.

http://dx.doi.org/10.1016/j.scitotenv.2022.155660
Received 22 February 2022; Received in revised form 28 April 2022; Accepted 28 April 2022
Available online 6 May 2022

permafrost and occurrence of fires. However, more sites with good chronologies are needed to thoroughly understand the spatial relationships between changing climate, permafrost degradation, and vegetation change, which ultimately affect the nomadic societies in the region of Central and Northern Mongolia.

1. Introduction

The current climate crisis and the associated abrupt processes are intensifying beyond the previously known framework (IPCC, 2018). The last decade witnessed a year-on-year increase in global temperature, with significant environmental and societal implications in each geographical region (Lenton et al., 2019). As a result of this warming trend, many positive feedback effects in the climate system resulted in regionally intensified hazardous droughts, fires, rainfall, or floods (Hessl et al., 2018; Payne et al., 2020; Pendergrass et al., 2020; Schoennagel et al., 2017). Unexpected rapid changes in the amount of precipitation or the uneven distribution of precipitation over seasons, together with the occurrence of prolonged heatwaves favoring droughts, put pressure on the environment (Graham et al., 2021; Van Loon et al., 2016). All these changes clearly indicate how the ecosystems of different climate zones reach their critical points and how their functional trajectories change over time. The status of ecosystems is reflected by their biodiversity, and depending on their composition and structure, ecosystems exhibit various degrees of resilience to climate changes and the ability to regain their prior functions (Falk et al., 2019; Ghazoul et al., 2015; Reyer et al., 2015).

One of the fundamental changes related to climate warming is the degradation of permafrost, which may accelerate carbon emission into the atmosphere (Biskaborn et al., 2019; Miner et al., 2022). It inspires also questions and studies related to ecosystems adaptations to permafrost changes (Harris et al., 2009; Turetsky et al., 2019, 2020). The shifts in atmospheric circulation and the resulting occurrence of heatwaves may have unknown consequences in areas of degrading permafrost (Dobricic et al., 2020; Perkins-Kirkpatrick and Lewis, 2020). One of them is the occurrence of extensive fires of boreal forest areas. For instance, the fires that occurred in 2018–2019 wreaked havoc on the environment on an unprecedented scale (Churakova Sidorova et al., 2020; Kelly et al., 2020; Kharuk et al., 2021).

Central Asia, especially Mongolia, has experienced extremely rapid climate changes in recent years (Hessl et al., 2018). It is reasonable to presume that the long-term rise in temperature and changes in precipitation resulted in significant shifts in the structure of the vegetation and an increase in the thickness of the active layer over permafrost (Hiyama et al., 2021). Severe fires have undoubtedly played a great role in these changes (Klinge et al., 2021a; Schneider et al., 2021). Northern Mongolia (the Khentii Mountains region) is on the southern margin of the boreal forest zone (Dashtseren et al., 2014), which is the second-largest contiguous forest zone (approximately 30% of the world's forested area) in the world and stores around 20% of the world's terrestrial carbon sink (Kuuluvainen and Gauthier, 2018). The forested area of Mongolia has over 123,000 km^2 of tree cover, which constitutes only 7.9% of the country's territory (http://portal.igg.ac.mn/dataset). Fire plays an important role in shaping the boreal forest ecosystems in Mongolia (www.globalforestwatch.org). According to the data from the Global Forest Watch, between 2001 and 2019 Mongolia lost up to 4350 km^2 of tree cover, which is equivalent to an 11% decrease (Curtis et al., 2018). Thickness of the active layer of permafrost and its discontinuous structure is very important element influencing the hydrology and vegetation composition of Mongolian landscapes, and consequently fires (Ishikawa et al., 2018). Rising temperatures, increased frequency and duration of droughts, and progressive permafrost degradation pose main challenges for the management of future habitats or the biodiversity of Northern Mongolia. However, there are still considerable gaps in our understanding of the processes associated with permafrost degradation in the past and the related ecological consequences. These relationships can explain the distribution of vegetation, the disappearance of permafrost, and shifts in fire regime in the Khentii Mountains region. Those links should be closely analyzed to understand the processes triggered by anthropogenic global warming and coexisting drought (Hessl et al., 2018; Ishikawa et al., 2018; Klinge et al., 2021a).

It is also necessary to determine the hidden relationships between the shifts in fire regime and the environmental consequences in Northeastern Mongolia. Therefore, we present the first high-resolution fire history from Northern Mongolia covering the last 1000 years, based on a multiproxy analysis of peat archive data (micro- and macroscopic charcoal, charcoal size classes and morphotypes, peat geochemistry). We used macroscopic and microscopic charcoal particles as a proxy for fire activity (e.g., Clark, 1988; Whitlock and Larsen, 2001), as well as pollen data to track the changes in regional and local vegetation compositions (Birks and Birks, 1980). We also performed a geochemical analysis to study the impacts of climate change and shifts in fire regimes on the functioning of the peatland ecosystem (Fiałkiewicz-Kozieł et al., 2016; Słowiński et al., 2016). Furthermore, we used the morphotypes of macrocharcoal to identify vegetation burning in order to better understand the shifts in past fire regimes and fire–vegetation relationships (Enache and Cumming, 2007; Walsh et al., 2017). The main goal of this study is to assess the role played by human behaviors, vegetation, and prolongated droughts on the occurrence of fire regime shifts in the last 1000 years in the permafrost marginal zone of Central Asia (Mongolia).

2. Study site and methods

2.1. Location of the study site and fieldwork

The Khar Zurkhnii Khukh Nuur (KHN) peatland is located in the Khentii Mountains range in Northeastern Mongolia and is about 200 km northeast of Ulaanbaatar (Fig. 1). The Khentii Mountains range is covered by a boreal forest and forest-steppe mosaic with discontinuous permafrost (Kopp et al., 2017) and has a diverse vegetation distribution. The main factors for influencing this variation are the exposition of the slopes and the associated occurrence of permafrost (Etzelmüller et al., 2006; Ishikawa et al., 2018; Schneider et al., 2021). Patches of permafrost can be found on the northern slopes and valley bottoms, and they play an important hydrological/ecological role in regulating local humidity and climatic conditions. Permafrost islands are overgrown by a dense boreal forest (Kopp et al., 2017; Lange et al., 2015) while the steppe vegetation with scattered shrubs predominates on the southern slopes without permafrost (Dashtseren et al., 2014; Kopp et al., 2017; Minderlein and Menzel, 2015). Mongolia has large south–north temperature gradients, and the average air temperature in the country ranges from −8 °C to 6 °C. In mid-January the lowest temperature of −34 °C occurs in the northern regions, and −20 °C in the southern regions (Dagvadorj et al., 2009). In the warmest months, the air temperature ranges between 10 °C and 15 °C in the northern territory and reaches 20 °C in the southern territory. The mean annual precipitation is 150–300 mm in the north and 50–100 mm in the south (Dagvadorj et al., 2009). Between 1960 and 2020, the mean annual air temperature in Mongolia increased by 2.4 °C (Dashtseren et al., 2021). According to the data from Global Forest Watch, fire season in the country usually starts at the end of March and lasts for about 16 weeks.

The studied KHN peatland is a typical rich fen dominated by sedges (i.e., *Carex cespitosa* and *Carex schmidtii*) with *Parnassia palustris, Equisetum fluviatile*, *Triglochin palustris* and brown mosses. In the central part the fen displays the hollow and hummock topography. The edges of the mire are occupied by a sparse population of willows and birches (*Betula humilis*). The mire has complex hydrology as the water supply changes seasonally, from snowmelt in the spring to precipitation in the summer. As a result, the water table in the mires fluctuates considerably throughout the year.

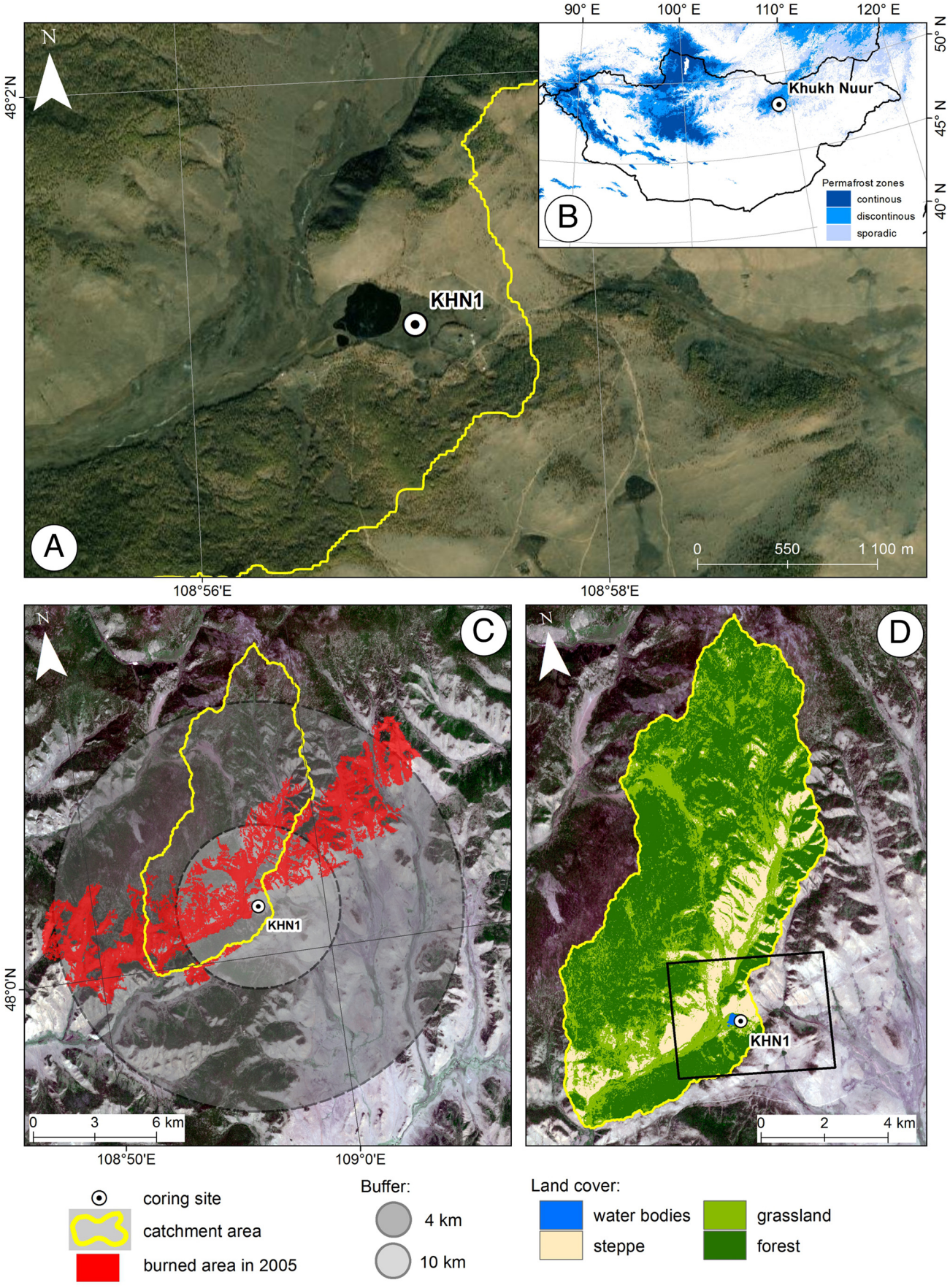

Fig. 1. Location of coring sites (A), the distribution of permafrost in Mongolia based on Obu et al. (2019) (B), spatial extent of the burned areas in 2005 based on Global annual Burned Area Map of 2005 (data comes from Long et al. (2019)), and (C) land cover in Mongolia from Sentinel-2 imagery using a supervised classification method (D).

The 36-cm-long KHN-1 peat profile was retrieved in summer 2017 using a long serrated knife (Fig. 1). The KHN-1 site is located in a peatland that has formed around the shallow lake "Khar Zurkhnii Khukh Nuur". Around the lake there is a gravel-sand dike which seems to be the rampart of a pingo scar (Fig. 1). However, the origin of the lake needs to be investigated further. The peat sequence has a thickness of ca. 40 cm, underlain by varigrained clastic sediments. The latter is still constantly frozen.

2.2. Laboratory analyses

2.2.1. Geochronology

The core chronology was based on combined analyses of short-lived radionuclides (^{210}Pb, ^{137}Cs) and AMS ^{14}C dating. Five samples of selected terrestrial plant macrofossils were collected from the KHN-1 core and were ^{14}C dated using accelerator mass spectrometry (AMS) in the Poznań Radiocarbon Laboratory (Table 1).

The last-century chronology of the KHN-1 core was established using ^{210}Pb and ^{137}Cs through gamma spectrometry. The samples of 1-cm-thick sediment core were dried and homogenized. Because the amount of samples available was small (<1 g), the adjacent samples were combined in some cases. The samples were packed into standard containers, sealed, and stored for at least two weeks before taking measurements. The activities of ^{137}Cs, ^{210}Pb, ^{214}Pb, and ^{214}Bi were measured for around 50–70 h, using a high-purity co-axial wide-energy germanium detector (Canberra GX2520), housed in the Institute of Geology, Adam Mickiewicz University in Poznań, Poland. The efficiencies of the measured geometries were determined using LabSOCS (Laboratory Sourceless Calibration Software) code and were verified using international radionuclide standards (IAEA-SL-2, IAEA-385, IAEA-447, IAEA-RGU-1). The average value of ^{214}Pb and ^{214}Bi, which are in radioactive equilibrium with ^{226}Ra, was considered a measure of supported ^{210}Pb ($^{210}Pb_{sup}$). The excess ^{210}Pb ($^{210}Pb_{ex}$), used for dating, was calculated as the difference between the measured total ^{210}Pb and $^{210}Pb_{sup}$ values. Based on the analytical results, an age model for the last century was developed using a the serac package (Bruel and Sabatier, 2020). The constant flux constant sedimentation (CFCS) rate and constant initial concentration (CIC) models were considered and were verified using the identified ^{137}Cs peaks. The absolute chronology was based upon five ^{14}C AMS dates (only terrestrial macrofossils were separated for ^{14}C AMS dates) provided by the Poznań Radiocarbon Laboratory (Poland) and ^{210}Pb dates described above (Table 1). The age-depth model was calculated using the OxCal 4.3 software (Bronk Ramsey, 2001).

2.2.2. Pollen analysis

The pollen composition (36 samples from KHN-1) was determined at a resolution of 1 cm. Pollen samples for the analysis were prepared by applying standard laboratory procedures (Berglund and Ralska-Jasiewiczowa, 1986) using *Lycopodium* markers to estimate the concentration of palynomorphs (Stockmarr, 1971). Palynomorphs were identified using photographic reference collections and keys (Beug, 2004; Faegri et al., 2000; Moore et al., 1991). At least 300–500 pollen grains of terrestrial plants (based on frequency) were counted for each sample. The sum AP + NAP (arboreal pollen and nonarboreal pollen) was calculated, except for the local aquatic and telmatic plants (*Cyperaceae, Sphagnum, Triglochin*). Zonation was confirmed by CONISS cluster analysis (Grimm, 1991), in which nonpollen palynomorphs and microscopic charcoal particles (>10 μm) were counted from the same slides as pollen.

2.2.3. Macrocharcoal analysis

The fire paleo record was obtained from 36 samples (each 2 cm^3) taken at 1-cm vertical intervals in peat profile. The collected samples were first bleached (Halsall et al., 2018; Hawthorne et al., 2018) and sieved through a 150-mm mesh. Charcoal particles with an size of >150 mm were counted using a stereomicroscope (Whitlock and Larsen, 2001). To account for variations in sedimentation in the sequence (Davis and Deevey, 1964), the macrocharcoal data were transformed into CHAR (charcoal accumulation rates or influx) by multiplying the concentrations of charcoal (particles/cm^3) with the sediment accumulation rates (cm yr^{-1}). In addition, based on their sizes, macrocharcoal particles were divided into three groups: 150–300, 300–500, and > 500 μm. The subdivision of macrocharcoal particles can provide information on the potential distance of fires from the studied site (e.g., Clark, 1988; Conedera et al., 2009; Vannière et al., 2008). On the other hand, the differentiation of two charcoal morphotypes (i.e., woody and herbaceous) allowed identifying the fuel sources for the fires. Woody particles were described as three-dimensional black and shiny block structures, and herbaceous particles originating from the above-ground parts of grasses, such as sedges and herbs, as two-dimensional elongated and structurally rich forms (Enache and Cumming, 2006; Mustaphi and Pisaric, 2014; Walsh et al., 2018).

2.2.4. Geochemical analysis

Prior to chemical analyses, and the samples were air-dried and homogenized using a Pulverizette 2 mill (Fritsch, Germany). The contents of total nitrogen (TN), total carbon (TC), and total sulfur (TS) of the samples were measured using a VarioMax CNS elemental analyzer (Elementar, Germany). The total inorganic (i.e., carbonate) carbon (TIC) content was determined via a two-step procedure involving combustion at 550 °C (4 h) and 950 °C (2 h), using the following formula:

$$TIC[\%] = 0.27 \bullet LOI_{950} = 0.27 \bullet \frac{100 \bullet (m_{550} - m_{950})}{m_{105}}$$

where:

LOI_{950} is the loss on ignition at 950 °C;
m_{550} is the mass of the sample combusted at 550 °C [g];
m_{950} is the mass of the sample combusted at 950 °C [g];
m_{105} is the mass of the sample dried at 105 °C [g]; and
0.27 is the conversion factor from CO_2 to C.

The total organic carbon (TOC) content was calculated as a difference between TC and TIC. The TOC/TN ratio was determined on a molar basis.

For the extraction of Fe, Mn, Ca, Mg, Na, K, and P, the samples were first combusted at 550 °C to remove organic matter and then treated with aqua regia (36% HCl + 65% HNO_3 (3:1, *v*/v); 12 h at room temperature followed by 2 h at 100 °C on a hot plate) using a reflux condenser. The residue remaining after combustion at 550 °C was considered as ash content (AC). The concentrations of Fe, Mn, Ca, Mg, Na, and K were measured by atomic absorption spectroscopy using a NovAA 300 device (Analytik Jena, Germany). The content of P was determined spectrophotometrically by LCK348 tests using a DR1900 device (Hach-Lange, USA). Samples were analyzed in duplicates. The accuracy of the analysis was verified using certified reference materials (Nonpolluted sediment (NPP) and Metals in sewage sludge).

Based on the bulk geochemical composition of KHN-1 core (AC, TOC, TIC, N, P, TOC/N, TOC/S, Fe/Mn, (Na + K + Mg)/Ca), the principal

Table 1
The P_Sequence depth/age model for the KHN-1 core.

Site (lab no.)	Depth [cm]	Material	F^{14}C ± 1 σ	^{14}C BP ± 1σ	cal CE ± 2σ	Comment
KHN-1 (Poz-105,986)	6.5	Macrofossils	106.97 ± 0.35		1956–1957	pMC
KHN-1 (Poz-105,984)	12.5	Macrofossils	117.58 ± 0.34		1993–1997	pMC
KHN-1 (Poz-105,985)	22.5	Macrofossils		100 ± 30	1683–1930	BP
KHN-1 (Poz-105,983)	30.5	Macrofossils		260 ± 30	1515–1800	BP
KHN-1 (Poz-105,989)	34.5	Macrofossils		995 ± 35	992–1157 CE	BP

component analysis (PCA) was applied on log-transformed data to delimit geochemical zones (GZ). Statistical calculations were performed using PAST software, version 2.17c (Hammer et al., 2001).

2.2.5. Statistical analysis

Patterns in the core data were identified using Kohonens artificial neural network (ANN), also referred to as a self-organizing map (SOM). The SOM analysis was performed on a data set comprising log-transformed abundances of 80 proxies (66 pollen taxa, AP, NAP, and 12 NPP taxa) sampled at 37 core depths (at 1-cm intervals).

ANNs are simple structural and functional brain models made of neurons (data processing units) grouped into layers. Compared to conventional analytical tools, these systems are advantageous for paleological research. The main advantage of ANNs is their resistance to noise in data (Lek and Guégan, 1999; Słowiński et al., 2018; Zhang et al., 2011). This is considered important due to the fact that the relationship between the real abundance of proxies and their abundance in paleoecological samples is distorted over thousands of years separating the living populations and their sampling. Moreover, regardless of time, the real abundances of populations are not often accurately reflected in samples (Ney, 1993; Płóciennik et al., 2015). The second advantage of ANNs is that they learn the model underlying the studied phenomenon directly from the data. Thus, these networks do not require a priori specification of the model by a researcher and can easily deal with the modelling phenomena described by variables that have nonnormal distributions and are related in a complex way (Brosse et al., 2001; Lek et al., 2005). Most proxies are linked by complex direct or indirect relationships, and their abundances mostly exhibit skewed distributions, making data normalization difficult due to a large number of zeroes in the data set (Quinn and Keough, 2002).

Kohonen's ANNs (SOMs) (Kohonen, 1982; Kohonen, 2001) are specifically used for classification purposes. In these networks, neurons are arranged in two (input and output) layers. The input layer acts as a flow-through layer receiving the data (Lek and Guégan, 1999). Because each input neuron receives information on one proxy, the number of input neurons equals the number of proxies (in this study 80).

The output layer is responsible for data structuring and output. Neurons of this layer create a two-dimensional grid (in this study 6 × 4). During Kohonen's ANN training, each output neuron repeatedly receives information from the input neurons. The intensity (weight) of signals sent from an input to an output neuron is modified (strengthened or weakened). A virtual core sample is thus created in each output neuron. The distance between the output neurons on the two-dimensional grid corresponds to the dissimilarity of respective virtual core samples. As a result, virtual core samples assigned to distant neurons differ significantly. Unless the neurons are in different clusters, the samples assigned to neurons located closer are similar. The clusters of output neurons (and the respective virtual core samples) can be distinguished using hierarchical cluster analysis (Ward linkage method with Euclidean distance measure) (Vesanto and Alhoniemi, 2000; Ward, 1963). Finally, each real core sample is assigned to the best-matching virtual core sample and the corresponding output neuron. Therefore, dissimilar real core samples are located in distant regions of the output layer, while similar samples are located in neighboring neurons or in the same neuron (Bae et al., 2014; Bedoya et al., 2009; Li and Vitt, 2013). Thus, Kohonen's ANN aids in recognizing the patterns in core samples and distinguishing their classes (Cheng et al., 2012; Lasne et al., 2007; Lek et al., 2005; Park et al., 2014).

Kohonen's ANN training was performed using SOM Toolbox (http://www.cis.hut.fi/projects/somtoolbox) (Vesanto et al., 2000). Using this package, the associations between each proxy and SOM regions (i.e., the distinguished stages of assemblage development) can be visualized as grayness gradients over the two-dimensional grid. Co-occurring proxies (including taxa with similar environmental preferences) usually have a similar pattern of grayness. However, the SOM Toolbox does not allow statistical verification of the associations, and hence, untransformed data were subjected to the Indicator Species Analysis, which is based on the indicator value (IndVal) (Dufrêne and Legendre, 1997). For example, an IndVal (%) of proxy *i* in all core samples of each subcluster *j* can be calculated as:

$$\mathrm{IndVal}_{ij} = \mathrm{A}_{ij} \times \mathrm{F}_{ij} \times 100$$

$$\mathrm{A}_{ij} = \mathrm{abundance}_{ij}/\mathrm{abundance}_{i}.$$

$$\mathrm{F}_{ij} = \mathrm{N\ core\ samples}_{ij}/\mathrm{N\ core\ samples}_{j}$$

where:

A_{ij} is the mean abundance of proxy *i* in the core samples of subcluster *j* divided by the sum of average abundances of the proxy *i* in all the subclusters (in this study 2),

F_{ij} is the relative frequency of occurrence of proxy *i* in the core samples of subcluster *j*, and

100 is a constant applied to obtain the percentages.

IndVal is maximum (100%) when all core samples with a given proxy are assigned to a single subcluster of output neurons and when the proxy is present in all core samples assigned to that subcluster (Dufrêne and Legendre, 1997). This parameter helps in identifying the proxies that are significantly associated within each subcluster of the real core samples, and thus complements the proxy SOM grayness gradient. In this study, the values of this parameter were calculated using PC-ORD statistical software (Mefford and McCune, 2011). The significance levels of IndVal for each subcluster of real core samples were determined using the Monte Carlo randomization test, which was also performed in PC-ORD software.

3. Results

3.1. Peat core properties and age–depth modelling

3.1.1. Core lithology

The 35-cm-thick depositional sequence consists of herbaceous peat with abundant sedges roots underlain by clastic substrate sediments primarily composed of sand. The latter sediments were still frozen. The boundary between the substrate and organic deposits at the depth of 35 cm was very sharp. The biogenic sequence was divided into two parts. In the upper part, with a thickness of 21 cm, single stems of *Sphagnum* mosses were found with brown peat characterized by a low degree of decomposition. The lower part, at the depth of 21–35 cm, contained the remains of brown mosses, with highly decomposed peat.

3.1.2. ^{210}Pb and ^{137}Cs dating

The vertical changes of $^{210}Pb_{ex}$ and ^{137}Cs is presented in Fig. 2, and the complete data set is available in the Supplementary File. Total ^{210}Pb and $^{210}Pb_{ex}$ activities showed a downward decrease, although with some irregularities (for instance, very low activities at the depth of 3.5–5.5 cm). These irregularities in $^{210}Pb_{ex}$ activity can probably be attributed to the very small amount of samples (<1 g) resulting in significant 2-sigma error bars; however, changes in the sediment accumulation rate could not be excluded (CIC model in Fig. 2). The activity profile of ^{137}Cs was characterized by a small near-surface peak (perhaps due to the 2011 Fukushima accident fallout), with high values at depths of around 9–10 cm (interpreted as 1986 Chernobyl peak), and maximum values at depths of 16–18 cm (likely due to nuclear weapon tests (NWTs) conducted in 1963 causing maximum fallout). Around 20-cm in depth, the activity of ^{137}Cs dropped to almost zero, which was interpreted as an indicator of the first fallout (FF) in the early 1950s. Below 20 cm, the activities of ^{137}Cs and $^{210}Pb_{ex}$ were very low which can be due to downward in-wash or mixing.

The age modelling performed for the upper 20 cm of the sediment core using short-lived radionuclides (Fig. 2) was primarily based on ^{137}Cs activity peaks (Chernobyl, NWT, FF) and adjusted CFCS model for $^{210}Pb_{ex}$ (several data points with negligible activities and/or significant 2-sigma uncertainties were ignored). The sediment accumulation rate determined for the upper 20 cm of the investigated core was approximately 3.16 mm

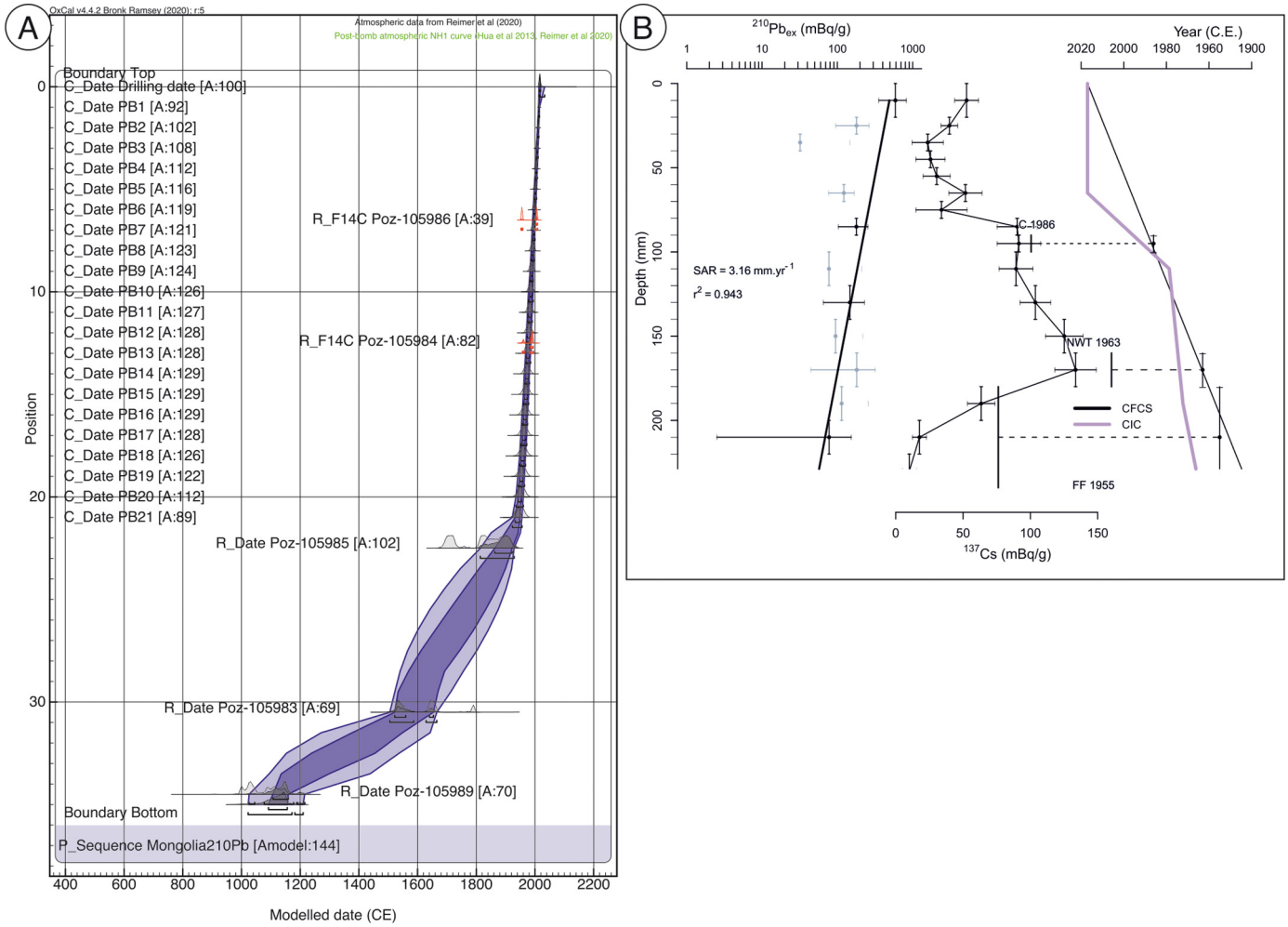

Fig. 2. Short-lived radionuclides measurements, and age depth model for KHN-1 core. a) age-model and ^{14}C results, and b) from left to right: ^{210}Pbex (semilogarithmic plot), ^{137}Cs, and the CFCS (constant flux constant sedimentation rate) and CIC (constant initial concentration) models. SAR – sediment accumulation rate, C 1986 – Chernobyl peak, NWT 1963 – Nuclear Weapon Test peak, and FF 1955 – First Fallout period. The vertical error bars refer to analyzed sediment sample thickness, while the horizontal bars depict 2-sigma uncertainty. The upper part (20 cm) of CFCS model, verified with ^{137}Cs activity peaks, was applied in further core age modelling. The figure was obtained in the R package (Bruel and Sabatier, 2020).

y^{-1}. The resulting model agreed well with the available postbomb ^{14}C dates.

3.2. Charcoal–fire regime history

The period between ca. 1000 and 1600 CE was characterized by low, decreasing upward values of CHAR (Fig. 3). This phase was dominated by herbaceous charcoals as well as woody particles. Between ca. 1600 and 1830 CE, when CHAR reached the lowest value, an increase in charcoal influx occurred. At ca. 1860 CE, a sharp rise in CHAR occurred, and the values remained high until ca. 1970 CE. In the followed period, the CHAR dropped again reaching the lowest values at ca. 1990 CE. Peak CHAR values, indicative of fires, occurred during the last few decades at ca. 1950 CE, ca. 1965 CE, ca. 1982 CE, ca. 2001 CE, and ca. 2014.

3.3. Pollen–vegetation changes

Pollen assemblage is the most potent proxy for reconstructing local and regional vegetation patterns or types as well as paleohydrological changes (Fig. 4; Table 2). Based on the pollen data from the last millennium, we identified five stages of development of local vegetation.

3.4. Geochemistry

The KHN-1 deposits were primarily composed of organic matter (represented by TOC) and detrital particles, represented by AC, with a small amount of carbonates (TIC content between 0.7% and 0.1%). The content of TOC increased upward throughout the core from 17% to 47%, while AC decreased from 67% in the bottom to 4% in the top of the core. Following a slight increase from 33 to 27 cm depth, TIC showed a decreasing trend above 27 cm. Statistical analysis revealed that the majority of geochemical variability (93%) of the sediments can be explained by two principal components (PCs), PC1 and PC2. PC1 explained 77.5% of the data variance and was strongly positively correlated to AC, TIC, and Fe/Mn ratio, and negatively correlated to TOC, TOC/TN, and TOC/TS (Table S1). PC2 accounted for 15.5% of the variance and was positively correlated to TN and total phosphorus, and negatively related to the ratio of (Na + K + Mg)/Ca (Table S1). Based on the stratigraphical variability of PC1 and PC2 (Fig. 5), the core can be sectioned into five geochemical zones (GZ). GZ1 was characterized by positive PC1 and negative PC2 values. In the GZ2 section, both PC1 and PC2 were positive and PC1 > PC2. In GZ3, both PCs were positive but PC1 < PC2. In GZ4 deposits, PC1 was negative and PC2 was positive. Negative values of both PCs were indicative of GZ5.

GZ1 (32–29 cm in depth) had relatively low TOC/TN (16–18) and TOC/TS (48–60) and high Fe/Mn (280–350). The value of (Na + K + Mg)/Ca

Table 2
Main features of local pollen assemblage zones.

Zone	Depth [cm] CE	Main features of local pollen assemblage zones
KHN_1–1 NAP-Pinus I	28.5–36 ca. 1000–1545	NAP grains reached above 50% (maximum 70%). *Artemisia* was dominant (46%). The share of Poaceae pollen increased from (3% to 15.7% top). Other herbaceous plants for which pollen grain share in this phase was higher than 1% were: Chenopodiaceae (3.1–6.4%), Ranunculaceae (0.8–3.1%), *Thalictrum* (1.3–3.6%), *Senecio*-type (0–1.4%), *Allium*-type (0–1.5%) but *Sanguisorba officinalis* less than 1%. Pollen grains of *Polygonum bistorta* regularly appeared. A few pollen grains of *Ephedra fragilis*-type and *Ephedra distachya*-type were also present. Among arboreal plants, the pollen grains of *Pinus* constituted the highest percentage (24.7–40.8%). The high share of tree pollen grains was found for the following: *Betula* (1.7–7.3%), *Larix* (0.6–6.1%), and *Salix* (0.2–2.4%). The only telmatic plants whose pollen grains were represented in this phase were Cyperacaeae (9.6–42.6%). A few coenobia of *Botryococcus, Spirogyra*-type, and *Zygnema*-type appeared in the bottom part. The top boundary of this zone was marked by increased NAP and decline in *Pinus*.
KHN_1-2 NAP	22.5–28.5 1545–1880	In this phase, NAP significantly increased and reached an absolute maximum of 79.2%. The main component was still *Artemisia* (36–53.3%) but its percentage was higher than in the KHN_1–1 phase. Chenopodiaceae (5.5–8.4%) and Poaceae (maximum 18.3%) were higher in the bottom but gradually decreased (to 7.5%) in the top part. In this phase, more taxa of herbaceous plants appeared, and the most important family were: Ranunculaceae (maximum 7.6% in the bottom and then declined), Apiaceae (0.8–2%), and Brassicaceae (0–0.8%). The continuous curves were still found for *Thalictrum* sp. (2.4–5.9%), *S. officinalis* (0.3–1.1%), *Senecio*-type, *Allium* sp., *P. bistorta*, and *Ephedra distachya*-type. Pollen grains of Cerealia cf. and *Rumex* sp. regularly appeared in this zone. The share of arboreal pollen grains decreased due to the decline in *Pinus* spp. The percentages of other main trees such as *Betula* and *Larix* were similar as in the previous phase. Only in this phase, single pollen grains of *Hippophae rhamnoides* appeared in the diagram. The share of telmatic plants was higher than in the lower zone. The values of Cyperaceae pollen grains doubled. The pollen grains of *Triglochin* and *Potamogeton*-type appeared in this zone. *Botryococcus* disappeared, but coenobia of *Zygnema*-type were still present. Top booudary of this phase was marked by a decline in NAP and an increase in *Pinus*.
KHN_1-3 Pinus	12.5–22.5 1880–1970	This zone was characterized by an absolute maximum of AP (71.4%). *Pinus* increased up to a maximum 60% and *Larix* reached a maximum 12.8%, while *Betula* decreased from its maximum of 7.3% to 1% at the top of this zone. The continuous curve of *Picea* appeared but its percentage was low (0.2–1%). NAP reached its minimum (28.6%) and was related to the main component of herbaceous plants, *Artemisia*, the pollen grains of which rapidly decreased in the bottom of the zone from 40.4% to 20.9% and then reached a value between 15.5 and 23.1%. The share of Chenopodiaceae was stable. The curve of Poaceae declined up to a minimum 1% at the top of the zone. *Thalictrum* reached maximum percentage in this phase (9.3%) and then gradually declined similar to *S. officinalis*. The curves of *Allium* sp. and *P. bistorta* and Cerealia cf. disappeared before the middle part of this zone. The curve of *Ephedra distachya*-type disappeared but this species was replaced by presence of *E. fragilis*-type pollen grains. Cyperaceae reached its maximum (69.6%), and a few spores of Filicales monolete and *Sphagnum* appeared in this zone. The continuous curve of *Triglochin* was still present but pollen grains of *Potamogeton*-type appeared occasionally. Chlorophyta was represented by *Zygnema*-type but coenobia of *Botryococcus* were noted additionally in the middle part of the phase. The curves of *Gelasinospora*, *Sordaria*-type, *Glomus*-type, and *Valsaria* cf. *variospora* appeared in this zone. The share of *Sordaria*-type and *Glomus*-type rapidly increased at the top of this LPAZ. The top boundary was marked by an increase in NAP and a decrease in *Pinus*.
KHN_1-4 NAP-Pinus II	3.5–12.5 1970 ÷ 2002	NAP increased and reached a value of 49.0–66.7%. This growth was caused especially by an increase in the percentage of *Artemisia* (approximately above 30%) and Chenopodiaceae (absolute maximum 11.9%). The share of Poaceae was variable (from 1.2% to 9.8%). The significant share in this phase were pollen grains of Ranunculaceae (3.1%), *Senecio*-type (2.6%), and Brassicaceae (3.1%) but their presence was discontinuously similar to *Thalictrum* (3.8%) and *S. officinalis* (2.3%). Pollen grains of *E. distachya*-type appeared alternately with grains of *E. fragilis*-type. A few pollen grains of Cerealia cf. were also noted. The decrease in the share of tree pollen grains was observed mainly for *Pinus* spp. but a downward trend was visible in the curve of *Larix* (10.6% in the bottom to 4.5% in the top part of the zone). The share of birch had an opposite trend increasing from 2.5% to 9.7%. Pollen grains of *Picea* appeared only in one sample in this phase. In the bottom part of the zone, the share of *Salix* increased to >1% but then its curve disappeared. The percentage of telmatic plants declined, the share of Cyperaceae pollen grains increased only at the top of the zone, and small spores of *Sphagnum* also appeared. In the middle part of this zone pollen grains of *Triglochin* disappeared. Non-pollen palynomorphs were represented by curves of *Gelasinospora* and very high percentages of *Sordaria*-type (maximum 27.7% and then declined till the top part of the zone), *Glomus*-type (gradually decreased in this phase from 24.6% to 6.3%), and *Valsaria* cf. *variospora* with two maxima (first in 11 cm depth (24.7%) and then in the top (5 cm depth) - 36.1%. The top boundary of the zone was marked by the decline in *Pinus*.
KHN_1-5 NAP-Betula	0–3.5 2002–2015	The decrease in *Pinus* share was associated with the increase in *Betula*. At the top of the core, the percentage of birch was the highest (28.7%). The share of *Larix* slightly decreased (2.2%). The share of NAP was similar to the previous phase and reached a maximum of 55.4%. The main components of NAP were still *Artemisia* (up to 34.1%), Chenopodiaceae (up to 9.3%), and Poaceae (up to 5.1%). The share of *Thalictrum* increased again (3.2%), similar to *S. officinalis* (1.7%). The pollen grains of Cerealia undiff. were present. A slightly higher value of Cyperaceae was noted, and the pollen grains of *Triglochin* returned. This zone was characterized by low values of *Gelasinospora, Sordaria*-type, and *Glomus*-type and a rapid decline in *Valsaria* cf. *variospora* curve.

was maximum (0.34–0.57) throughout the core. P increased slightly from 0.23 to 0.32 mg·kg^{-1}. GZ2 (29–19 cm) was marked by maximum values of Fe/Mn, with the content of nutrients increasing upward. At the same time, TIC, AC, and (Na + K + Mg)/Ca showed a declining trend from bottom up. The ratios of TOC/TS and TOC/TN were similar to those in GZ1. GZ3 (19.0–9.5 cm) showed a considerable upward decrease in Fe/Mn, accompanied by s in TOC/TN and TOC/TS ratios. On the other hand, TIC and (Na + K + Mg)/Ca were low, while nutrients were at their maximum with slight variations. GZ4 and GZ5 constituted the upper part of the core. The former was represented by two thin intercalations at 9.5–8.5 and 7.5–6.5 cm and acted as a transition zone between GZ3 and GZ5. The transition from GZ3 and to GZ4 was marked by a very sharp increase in TOC/TN and TOC/TS ratios as well as a decrease in TIC. Between 9.5 and 6.5 cm, a steep decrease in N and P was noted and TOC/TN and TOC/TS showed minor variations with a tendency toward lower values in GZ4 deposits. TOC/TN and TOC/TS ratios varied slightly and reached lower values in GZ4 deposits. A continuous GZ5 commenced at 6.5 cm. In this zone the maximum contents of TOC and TOC/TS and TOC/TN values were accompanied by the minimum shares of AC, TIC, nutrients, (Na + K + Mg)/Ca and Fe/Mn.

3.5. Kohonen's artificial neural network

Two main clusters of output neurons, X and Y, were distinguished in Kohonen's ANN (Fig. 5). Cluster X was composed of subclusters X1 (i.e., neurons D3, D4, E3, E4, F3, and F4) and X2 (D1, D2, E1, E2, F1, and F2), whereas cluster Y was composed of subclusters Y1 (A4, B3, B4, C3, and C4) and Y2 (A1–A3, B1, B2, C1, and C2) (Fig. 5).

A temporal gradient was clearly visible in the sequence of subclusters X1–Y2, reflecting the stages of assemblage development. The first stage was X1 (corresponding to the deepest samples from the core depths of 36–30 cm). Then, the assemblage passed to the X2 stage (29–22 cm), temporarily reverting to the X1 stage (at 25 and 22–19 cm). The next stages, Y1 (18–14 cm) and Y2 (13–03 cm), were stratigraphically constrained. Finally, the assemblage returned to stage X2 (the three shallowest samples) (Fig. 5).

A total of 22 proxies (i.e., >27% of those used for the SOM classification) were associated with certain SOM subclusters (Fig. 6). There were 14 plant taxa, AP, NAP, four fungi, one protist, and one animal (Fig. 5). The highest number of indicator proxies were identified for subclusters Y1 (8) and X2 (7), and the lowest for X1 (2). The number of indicator proxies identified for Y2 was 5 (Fig. 6).

4. Discussion

4.1. Ecological interpretation

4.1.1. KHN-1 phase (ca. 1000–1545 CE)

The development of KHN mire, which dates to ca. 1000 CE, seems to be associated with the improvement of climate in North Mongolia in the Medieval Warm Period (MWP; first half of the 11th century; Davi et al., 2015). That was when the pingo likely collapsed. It is common, as stated by Mackay (1998), that the pingo collapse may result in the formation of shallow thaw depressions/ponds at its upper part, with changing surface area and water depth with progressive thawing. The identified possible pingo ramparts around the study site suggest that the KHN lake /mire was located in such a depression. A high share of Cyperaceae pollen and TOC/TN ratios of 16–18, typical of sedges (Szajdak et al., 2020), in the bottom section of the core indicate that the site has been occupied by sedge fen since the onset of the peat accumulation process. The peat accumulating in this fen was relatively low in TOC and enriched in AC. The mineral matter presumably originated from ambient slopes (i.e. solifluction, slumping of permafrost active layer) as inferred from the high values of (Mg + K + Na)/Ca ratio (Klinge et al., 2021b) (Fig. 5). During the early stages of KHN evolution, the peat accretion was very slow and proceeded at a rate of approximately 0.1 mm yr^{-1}. A low peat accumulation rate has been reported for permafrost sites (Loisel et al., 2014); however, the arid climate of MWP in Mongolia (Dugerdil et al., 2021; Lan et al., 2018) could also affect peat formation, which is known to be partially controlled by water availability (Charman et al., 2013). The inclusion of coenobiae of *Botryococcus* in the pollen record highlights that the conditions were favorable for the growth of green algae in the mire, thus proving the high water level therein (Jankovská and Komárek, 2000; Komárek and Marvan, 1992; Shumilovskikh et al., 2021). This interpretation is further supported by the presence of *Salix*, which is known to tolerate damp soils and flooding, as well as plants associated with moist sites, such as Ranunculaceae (*Ranunculus acris*-type), *Thalictrum, Polygonum bistorta*, or *Sanguisorba officinalis*. In addition, a high Fe/Mn ratio indicates the low oxygenation of the mire waters, certainly due to inundation (Schlütz et al., 2008; Zarzycki et al., 2002). Peat that accumulated in oxygen-free conditions is poorly decomposed, as evidenced by a low TOC/TS ratio (Fig. 5). The predominance of steppe plant communities in the vicinity of a developing mire was evidenced by >50% frequency of herbaceous pollen grains represented by Asteraceae (*Senecio*-type, *Matricaria*-type), Caryophyllaceae (*Silene*-type, *Gypsophila*-type), *Campanula*, and *Scabiosa*, as well as a high share of *Artemisia.* The results of Indicator Species Analysis revealing significantly highest occurrence of *Allium* and *Thymelaea* pollen types in the SOM phase X1 (Fig. 6), and additionally the presence of *Matricaria* pollen types, indicate distinct habitat conditions of this period associated with meadow and steppe vegetation. The latter pollen types most likely represents one of the genera of the Thymelaceae family (*Diarthron*), the occurrence of which has been confirmed by botanical studies (Virtual Guide of the Flora of Mongolia). All these taxa can be combined in open vegetation with lower humidity requirements. The above indicator taxa (i.e., those with statistically significant IndVals) should not be necessarily regarded as dominants. They indicate particular edaphic and climatic conditions of phase X1 that were more favorable for them than all other phases. Although trees occurred in the landscape, the majority of AP probably originated from the light taiga forest, with *Pinus sylvestris*, *Larix*, and *Betula* growing primarily on the mountain slopes. Based on the occurrence of *B. humilis* in the vicinity of the lake adjacent to the mire (field observation), it can be assumed that this species was locally present in the fen during the initial phase, which is in line with its moisture preferences (Zarzycki et al., 2002). A high abundance of charcoal remains, predominantly of size 150–300 μm, confirms fire activity in the vicinity of the KHN site. However, owing to the very low values of CHAR (4.3 particles·cm^{-2}·y^{-1}) and amalgamation of the depositional record, a reliable reconstruction of the fire history of the area for that time period is difficult (Mooney and Tinner, 2010).

4.1.2. KHN-2 phase (ca. 1545–1880 CE)

This phase was largely influenced by the Little Ice Age (LIA, ca. 1545–1880 CE) period, the most severe cooling period during the last millennium (Bader et al., 2020). During this period, the percentage of herbaceous pollen, particularly those of Poaceae and *Artemisia*, increased by up to 80%. Furthermore, other steppe species such as *Bupleurum* or *Pulsatilla* (Gunin et al., 1999; Schlütz et al., 2008), were more abundant. *Ephedra* (especially *Ephedra distachya*-type) also increased considerably, indicating an environment of sparse vegetation. The frequency of AP grains reached the lowest values during the last millennium. These paleobotanical data suggest that the light taiga forests retreated and the landscape became more steppe in nature than in the preceding phase. Only the frequency of birch increased slightly, presumably owing to its tolerance to climate deterioration. The plant taxa that the Indicator Species Analysis indicated as distinguishing the habitat (SOM phase X2) were found in both open (steppe) communities (mostly NAP) representing regional vegetation and the plant communities related to moist environments (*Potamogeton*-type) of the mire (Fig. 6). This can be associated with the climatic conditions prevailing during the LIA. Climate cooling in this period could have enhanced permafrost aggradation, thus decreasing the permeability of local soils (Hahn et al., 2013). On the other hand, some evidence indicates an increase in humidity in Central Asia during the LIA (Chen et al., 2006; Dugerdil et al., 2021; Lan et al., 2018; Putnam et al., 2016; Yao et al., 2020). Enhanced surface runoff and restricted water infiltration to deeper layers of frozen soils (Hahn et al., 2013) together resulted in a high level of groundwater and thus low redox conditions in the KHN site, as revealed by high Fe/Mn values (Boyle, 2001) as well as the appearance of palustrine and open water plant sporomorphs such as marsh arrowgrass (*Triglochin*), *Potamogeton*-type pollen, and *Ceratophyllum* spine. Consequently, the peat accumulation rate of approximately 0.24 mm·yr^{-1} was relatively high, and the peat was characterized by low decomposition as well as TOC enrichment (21–33%). The contribution of AC was still important, consistently with the predominant role of surface runoff in the mire hydrology. It is known that nutrients are released during soil leaching (Żarczyński et al., 2019). This could explain the increase in the contents of P and N throughout the the LIA deposits, indicating the fertile nature of the mire and favorable growth conditions for sedges (Hinzke et al., 2021). The considerable role played by sedges in the KHN mire during LIA was confirmed by a sharp increase in Cyperaceae pollen at the onset of this period as well as by the TOC/TN ratio of 16–18, which is typical of sedge peat (Szajdak et al., 2020). Slightly enhanced TIC content confirmed that the fen water had neutral or mildly alkaline pH. During this phase, micro- and macrocharcoal contents, as well as CHAR, were generally low in the peat. Their presence justifies the conclusion of a low fire intensity during the LIA, in line with the regional reconstruction by Hessl et al. (2016). The diminished fire activity was fuel-limited, and the most plausible reason was the low biomass of herbs and woody plants.

4.1.3. KHN-3 phase (1880–1970 CE)

The climate of Central Asia has been showing a warming trend since the late 19th century (Chen et al., 2006; Davi et al., 2015; Yao et al., 2020). The increase in air temperature was accompanied by a decrease in humidity (Chen et al., 2006; Putnam et al., 2016), however there are also contrary reconstructions providing evidence for a change toward more humid conditions (Yao et al., 2020). Heatwaves have become a common climatic event, with one of their major effects being the occurrence of unprecedented, prolonged droughts (Erdenebat and Sato, 2016; Hessl et al., 2018). The increasing frequency of heatwaves resulted in diverse and complex feedback mechanisms leading to changes in ground moisture level and thickness of the active layer over permafrost, as well as fires, which ultimately affected the nomadic societies in the region (Dangal et al., 2016; Hiyama et al., 2021). Some of these changes can also be identified in the peat record from the KHN site. During the KHN-3 phase, profound environmental changes occurred in the mire and its surroundings. The stable (albeit slightly higher compared to the LIA) TOC/TN ratio of 17–19 and the highest share of Cyperaceae indicated that the mire was still dominated

by sedges. In addition, the high contents of N and P suggested the high fertility of the mire which was favorable for sedges (Hinzke et al., 2021). However, after the termination of LIA, AC and (Mg + K + Na)/Ca decreased in the mire, accompanied by a steep upward decrease in Fe/Mn ratio. The former reflects a minor role of allochthonous material and can be linked to climatically induced partial reforestation of the catchment as indicated by the increase in the AP/NAP ratio (Fig. 4). The decrease in Fe/Mn ratio signifies the shift from reducing toward more oxidizing conditions in the mire, which plausibly resulted from the lowering of the groundwater table. The water level changes may be seen as a direct or indirect response of the mire to more arid climate of the post-LIA period. In some regions of Central Asia, drying has resulted in a remarkable decrease in lake levels (e.g., Putnam et al., 2016). However, at the same time in some W Mongolian lakes the water level has risen (Unkelbach et al., 2019). This was attributed to the degradation of permafrost and thus showed regionally diverse environmental responses to post-LIA climatic changes in Mongolia. According to Mackay (1998), the lowering of water level in the post-pingo wetlands may be caused by the drainage of the thawing pond via dilation cracks in the pingo ramparts. As such, the decrease in groundwater level at the site could have resulted from climatically controlled reactivation of the pingo collapse during the post-LIA climatic amelioration. Drainage of the mire led to peat degradation. The slight upward rise in TOC/TS ratio indicates that the process of peat decomposition was accelerated during the KHN-3 phase. The increased TOC/TS ratio is usually linked to the preferential loss of sulfur from the solid phase of peat during its decomposition under oxidizing conditions (Eimers et al., 2003) (Fig. 5). As previously stated, the period between 1880s and 1950s was marked by the reestablishment of forest in the KHN neighborhood. Pollen record reveals a high increase in *P. sylvestris*-type, *Pinus-Haploxylon*-type (in this area, it can refer to *Pinus sibirica*) (Schlütz et al., 2008) and *Larix*, with a marked presence of *Picea*, thus indicating the predominance of the light taiga-type forest with pine and larch, which are typical in the lower mountain belts. However, in the upper part of the mountains, dark taiga with Siberian pine and spruce could occur locally (Schlütz et al., 2008). This period of the highest forest development in the area terminated around 1970 CE just after the end of AP. Despite the decline in herbaceous taxa, *Ephedra* pollen (mainly *Ephedra fragilis*-type) was still present, implying that habitats adjusted to drier conditions and poor vegetation cover. At the same time, the conditions were favorable for mire development and both *Triglochin* and Cyperaceae were abundant. Furthermore, the high moisture on the mire is evidenced by the presence of green algae, such as *Zygnema*-type and *Botryococcus*, and single pollen grains of *Potamogeton*-type. The results of the SOM analysis suggested that this phase can be divided into two based on the appearance of some nonpollen palynomorphs in the sediments. The period before the 1950s, marked as X1, shows similar environmental conditions as before LIA, with open plant communities still dominant. The next SOM phase, Y1, refers to warming and changes in vegetation cover (maximum forest area). Habitat changes that occurred after 1950 are indicated in the Indicator Species Analysis by the significantly highest IndVals of woody species (generally AP), as well as of ascospores of the carbonicolous fungus *Gelasinospora* and oocytes of *Rhabdocoela* (Turbellaria) (Fig. 6). The large increase in biomass and the increased number of tree stands present, which were most likely related to the change of landscape to forest-steppe, resulted in the intensification of fire (Klinge et al., 2018). This is evidenced by an increase in the abundance of microcharcoal and CHAR as well as by the increased number of *Gelasinospora* fungi in the peat. The latter is associated with charred material and more dry conditions (Shumilovskikh et al., 2021; van Geel and Aptroot, 2006). Interestingly, the enhanced fire activity in the KHN mire and its vicinity contradicts the reconstruction by Hessl et al. (2018) who concluded that fires in Mongolia wanned in the mid-20th century. Peat accumulated between 1950 and 1970 showed the presence of the first ascospores of fungi (*Sordaria*-type) and genus *Valsaria* cf. *variospora*. The proportion of fungi rapidly increased vertically. *Sordaria*-type fungi are known to be coprophilous (Shumilovskikh et al., 2021; Tian et al., 2014; van Asperen et al., 2021), and their occurrence can be linked with the intensification of pastoral farming in the studied area. Mandel (1949) highlighted that Mongolian natives have always lived a nomadic cattle-raising lifestyle, with their private farms including up to 5000 sheep, cows, camels, and horses. In the 1930s and 1940s, several agricultural reforms were implemented to mitigate the problems caused by droughts and late harsh winters with heavy snowfall. As a part of the plan to prevent drought, around 22,000 wells were dug during the 13 years from 1932 to 1945. An important element affecting the cattle population is the availability of pasture during the winter. In the winter of 1944–1945, the pastures were covered with a thick layer of snow, restricting access to pasture, and resulting in the death of over a million cattle, a phenomenon known as deadly dzud (Mandel, 1949). As Fernández-Giménez et al. (2017) underlined, during the communist collective era a dynamic growth of livestock was observed from 1924. According to the data from the Information and Research Institute of Meteorology, Hydrology and Environment in Mongolia, more severe and frequent dzuds are expected in the future (Fig. 7). The observations of the Institute indicate that dzud occurs cyclically at intervals of several years to even a decade (1944–1945, 1967–1968, 1978–1979, 1999–2002) (Punsalmaa, 2006). The most severe dzuds were observed in the winters of 1999–2002 and 2009–2010 resulting in the death of more than 21.5 million livestock (Mongolian Statistical Information Service, www.1212.mn). Nevertheless, we consider that this phenomenon was also present in the past but not on such a large scale as a result of the communist collective policy (Fernández-Giménez et al., 2017; Mandel, 1949). Lehmkuhl et al. (2011) underlined that grasslands are characterized by their fire behavior but on the other hand they found no evidence for frequent paleo-fires in Mongolia, pointing out that livestock grazing had eliminated most of the fuels necessary to sustain a fire (Umbanhowar et al., 2009). Many authors argue that past changes in vegetation are a direct reflection of changes in climate (Chen et al., 2008; Tian et al., 2017).

4.1.4. KHN-4 phase (1970–2005 CE)

After 1970, the AP/NAP ratio decreased (Fig. 4), indicating the shrinkage of forest in the region. As revealed by the pollen data the shares of *P. sibirica* and *Picea* declined, while Scots pine and larch became the main forest components. Herbaceous taxa (both terrestrial and telmatic) decreased in number, and a few pollen spectra (pollen samples) reached the lowest abundances (Fig. 4) (only 7–8 taxa were present). In addition, the lowest concentration of total pollen grains was noted at the core depth of 5–10 cm (1982–1998 CE). On the one hand, these features point to the unfavorable conditions for the preservation of palynomorphs (e.g., oxidizing conditions in peat), and on the other hand, it is associated with an increase in the sedimentation rate (e.g., Berglund and Ralska-Jasiewiczowa, 1986). A rapid decline in Cyperaceae at the point of transition from KHN-3 to KHN-4 marks a substantial change in local plant community and peat-forming processes. This is also signaled by a decreased Fe/Mn ratio which indicates the shift toward higher peat oxygenation, and presumably results from the lowering of the ground water level. The disappearance of *Triglochin* and subsequent occurrence (albeit in low amounts) of *Sphagnum*, *Habrotrocha angusticollis,* and *Gelasinospora*, as well as large numbers of *Assulina muscorum* shells, support the development of relatively dry habitat on the mire (Andrews et al., 2021; Shumilovskikh et al., 2021; Stivrins et al., 2019; Warner and Chengalath, 1988). An immediate effect of hydrological changes in the mire was accelerated peat decomposition as indicated by the increase in the TOC/TS ratio (Eimers et al., 2003). The spread of *Sphagnum*, and its apparently greater contribution to the biomass in the KHN peat, was responsible for the increased TOC/N ratio observed in the mire (Szajdak et al., 2020; Zibulski et al., 2017). Although the mire was relatively dry, the fires were generally uncommon, and the frequencies of charcoal particles and CHAR thus remained low during KHN-4. However, a positive trend in the abundance of both charcoal particles and CHAR was observed around the end of the 20th century (Fig. 3). It is presumed to be a record of widespread fires in Mongolia stimulated by droughts and reduced soil moisture (Hessl et al., 2016). The reasons for the suppressed fire activity are unclear because the KHN-3 phase is mainly marked by severe drought in Mongolia (Hessl et al., 2018). Based on this coincidence, more frequent fire activity could be expected. Therefore, we base our interpretation on

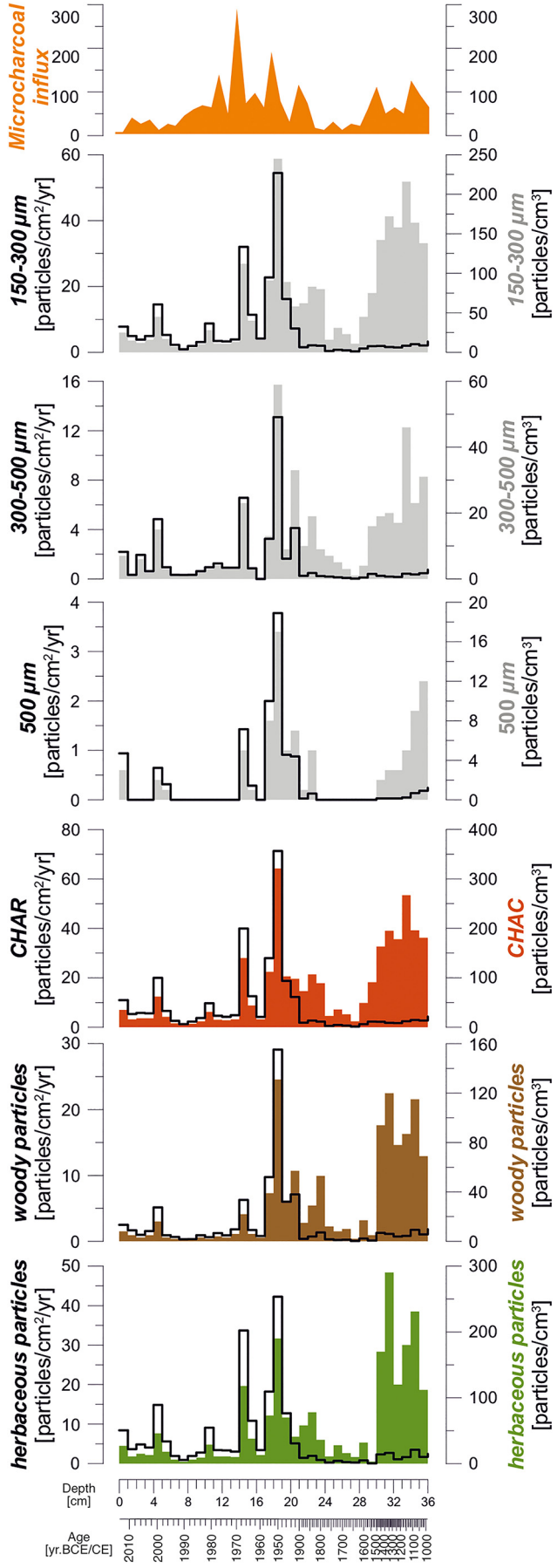

Fig. 3. Charcoal distribution (influx [CHAR, particles/cm^2/yr] and concentration [CHAC, particles/cm^3]) in the KHN-1 core. Two morphotypes (herbaceous vs woody) and three charcoal size fractions (150–300, 300–500, and > 500 µm) were distinguished.

the hypothesis by Hessl et al. (2016) that the frequency of fires is associated with the intensity of grazing. It appears that intensive grazing greatly reduces the availability of flammable plant biomass, effectively cutting fires off from fuel resources. The highest abundances of *Sordaria*-type and *Valsaria* cf. *variospora,* fungal species found on animal dung and eutrophic habitats, respectively (van Geel and Aptroot, 2006), identified in the KHN-4 record provide strong evidence for intensive grazing on the mire and its surroundings. During the terminal part of the KHN-4, corresponding to ca. 1990–2005 CE, the physicochemical conditions of the mire changed substantially. A sharp increase in the TOC/TN ratio (up to >40) suggests the dominant role of brown and/or *Sphagnum* mosses in the peat-forming processes (Szajdak et al., 2020; Zibulski et al., 2017), and thus implies a more ombrotrophic character of the mire. The extremely low TIC content, indicating acidic conditions in peat, supports the hypothesis on primarily atmospheric water supply. Very low Fe/Mn values point to a predominantly oxidizing environment, and thus a low water level. The latter created favorable conditions for peat degradation, and a high degree of degradation was confirmed by a very high TOC/TS ratio. Interestingly, the upward decline in P and N indicates low nutrient availability and can be explained by nutrient loss associated with peat degradation (Bragazza, 2008). The changes in the mire seem to be influenced by climate because the mire processes coincided with amplified warming and severe drought, shaping the climate in Mongolia since the mid-1990s (Hessl et al., 2018).

4.1.5. KHN-5 phase (2005–2015 CE)

Geochemical data revealed that during the KHN-5 phase only minor environmental changes occurred on the KHN mire and in the adjacent forest-steppe landscape. However, a several-fold increased frequency of birch pollen grains clearly demonstrated the encroachment of *Betula* sp. (*humilis*) shrubs on the mire. Trees colonize mires for a variety of reasons, including landscape transformation, climate, and fires (Beauregard et al., 2020). Our data set is insufficient to fully explain this issue. It seems, however, that both climatically induced water table decrease and fire episode around 2000 CE favored the survival and germination of *Betula* seedlings on the mire. Weak pression from trampling and grazing by cattle, as corroborated by significantly reduced shares of *Sordaria* (Fig. 4), could also aid in the spread of *Betula*. The appearance of birch was presumably not without significance for biogeochemical processes in peat. Koretsky et al. (2006) demonstrated that higher vegetation tends to leak oxygen into the rhizosphere thus creating oxic microzones in the subsurface peat layers. The plant-mediated oxygen transfer might have been the reason for the low Fe/Mn ratio during the KHN-5 phase and, because in oxidizing conditions the degradation of the peat substrate was enhanced, it ultimately led to the high TOC/TS and TOC/TN values (Fig. 5). The results of the SOM analysis again indicated a phase X2 (Fig. 5), suggesting that the modern environmental conditions are similar to that during the LIA and characterized by abundant steppe (open communities) vegetation (Fig. 4), with high shares of all terrestrial herbaceous plants (NAP), Poaceae, and *Artemisia.* The significant association of *Potamogeton*-type with the phase X2 (Fig. 6) also revealed the moisture conditions on the mire, which are additionally marked by the curve of *Triglochin* and a high percentage of Cyperaceae in the pollen diagram. After 2005 CE, the ascospores of all fungi types decreased significantly.

4.2. How to understand "dzud"—droughts, snow, and fires

According to Hessl et al. (2018), the 20th century was one of the warmest periods in Mongolia during the last 1200 years. The warming has multiple environmental implications among which degradation of permafrost seems to be the most vital, however the climatically-induced changes in permafrost in Mongolia are still poorly understood (Dashtseren et al., 2021). Recent study by Hiyama et al. (2021) suggest

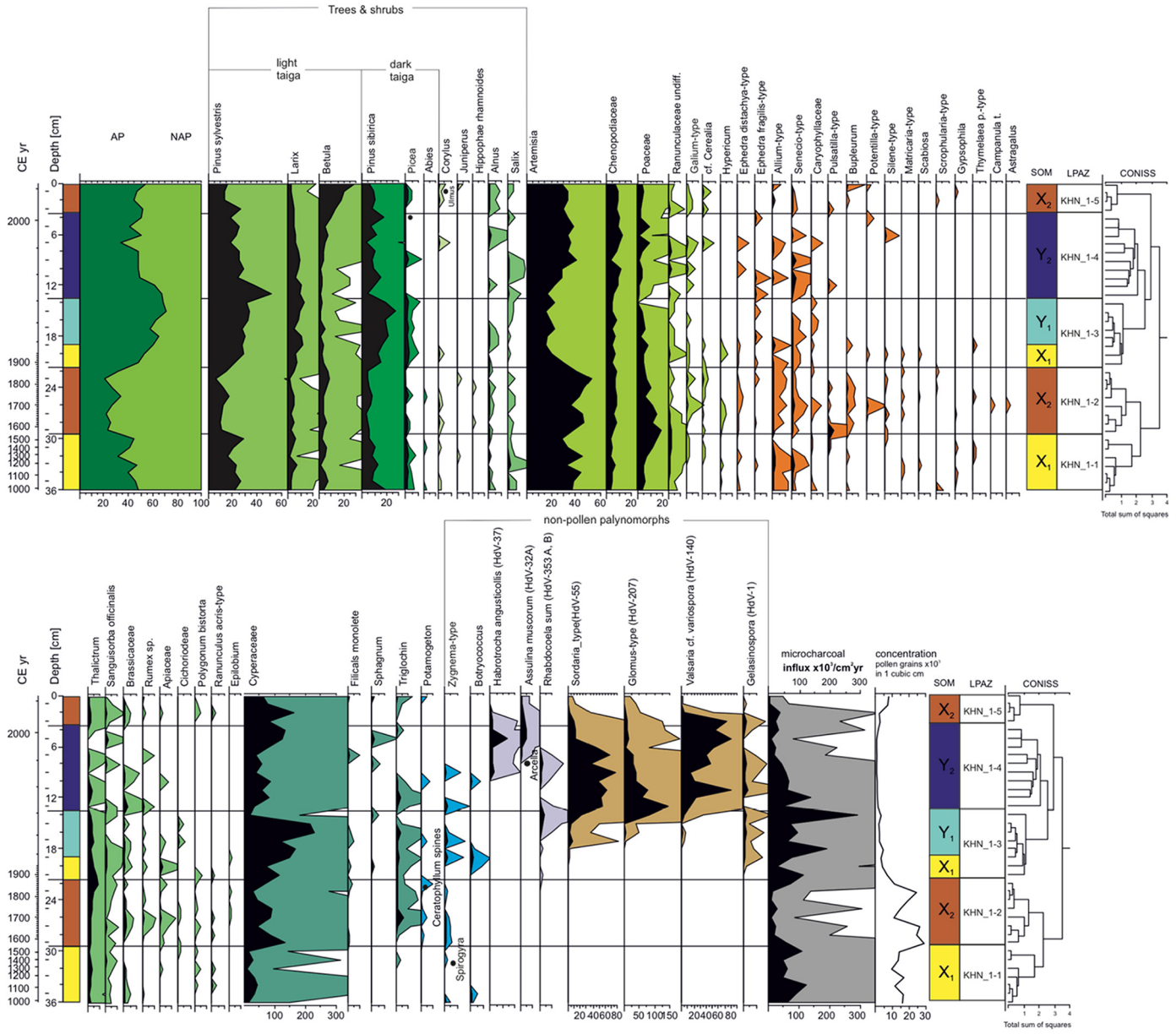

Fig. 4. Pollen diagram for the Khar Zurkhnii Khukh Nuur (KHN-1).

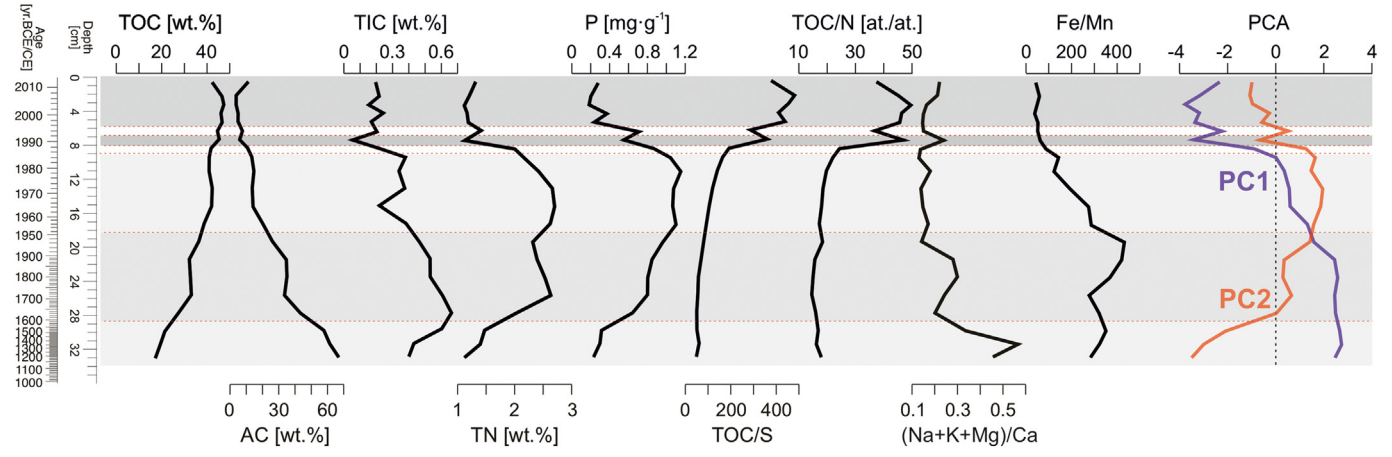

Fig. 5. Geochemical composition of the sediments and PCA axes 1 & 2.

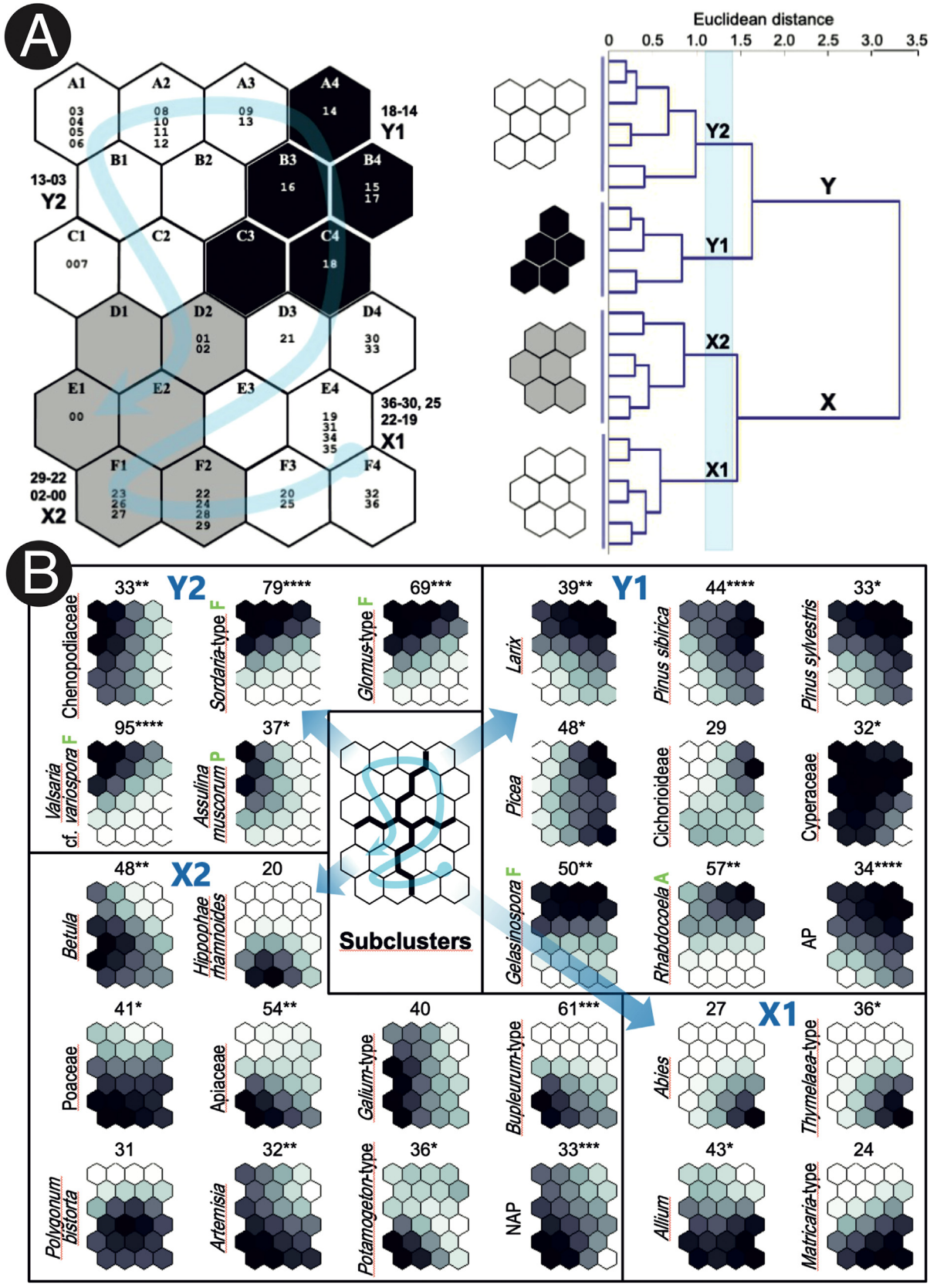

Fig. 6. (A) Real core samples, from 37 core depths (in cm), assigned to 24 self-organizing map (SOM) output neurons (A1–F4) arranged into a two-dimensional grid (6 × 4). Clusters (X, Y) and subclusters (X1, X2, Y1, and Y2; shown in different degrees of grayness) of neurons and respective virtual core samples have been identified with the use of hierarchical cluster analysis. A core-depth range is presented above each subcluster symbol; (B) Twenty-eight proxies associated with SOM subclusters (X1–Y2) at $p \leq 0.1$. AP – arboreal pollen, NAP – nonarboreal pollen; A – animal, F – fungus, P – protist. The shading (darker for a stronger association in virtual core samples) is scaled independently for each proxy. The maximum observed indicator value (IndVal; shown above each proxy plane) and the significance level (**** $p \leq 0.0001$; *** $p \leq 0.001$; ** $p \leq 0.01$; * $p \leq 0.05$) were calculated on the basis of real core samples.

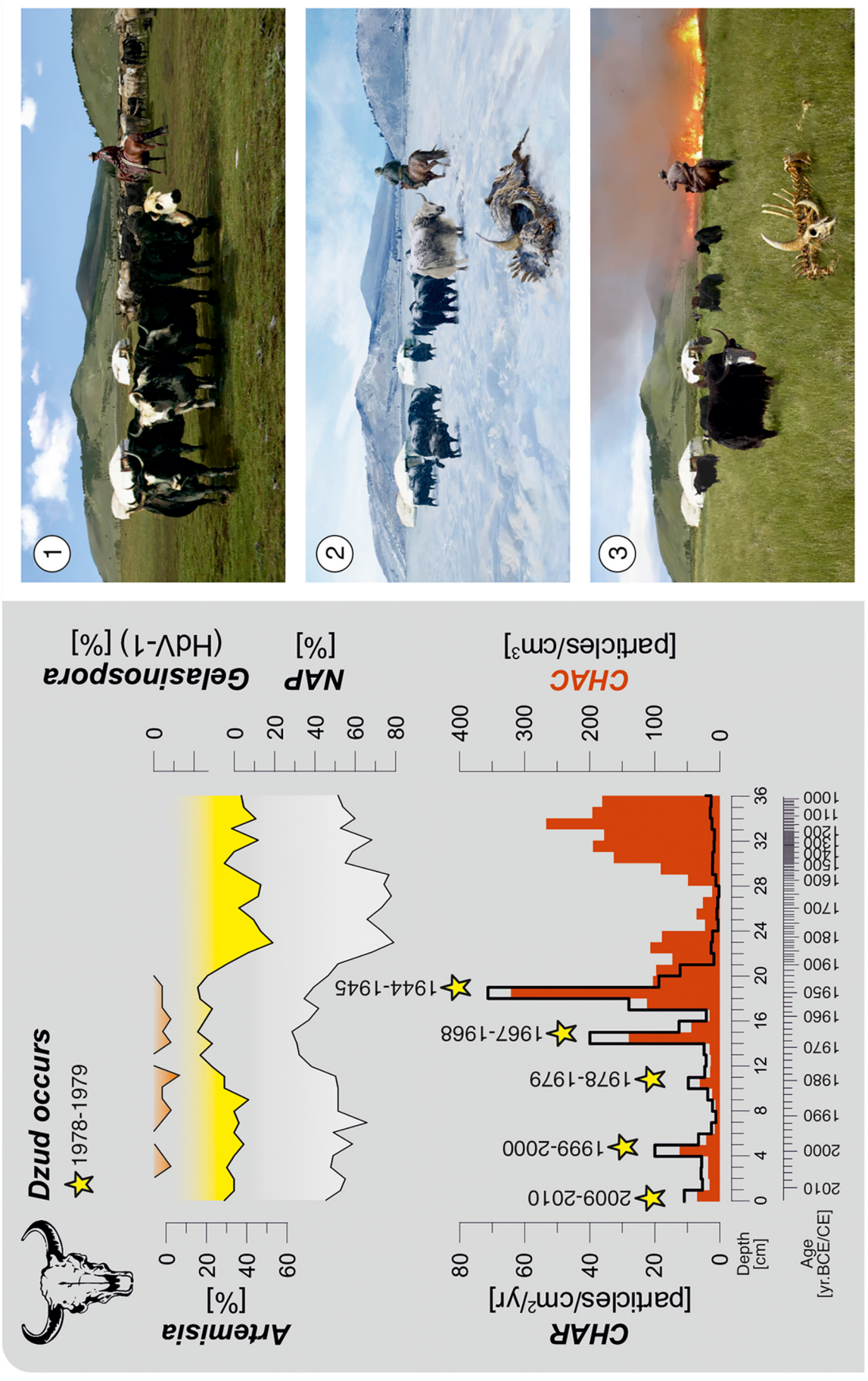

Fig. 7. Relationship between the occurrence of severe "dzud", vegetation and fire's episodes in the history of Mongolia. 1) Occurrence of drought during the summer; 2) harsh and snowy winters leads to starvation and mass die-offs of livestock; 3) after the snow has melted, most of the dry biomass becomes fuel for the spring fire. Illustrations of the three phases were drawn by Tomasz Rygier.

that rising air temperatures and gradual thawing of permafrost in the region cause deeper circulation of groundwater, thereby activating more productive springs.

Our results suggest that another effect of climate change in Mongolia can enhance fire activity. From the KHN record it emerged that during the Anthropocene there were at least five episodes with extensive fires in Mongolian steppe (Fig. 7). According to the Global Forest Watch the fire season that in Mongolia is usually between spring and summer and begins around the end of March and lasts for nearly 16 weeks. In addition we found that the fire episodes were coincident with dzud, the regional phenomenon of mass die-offs of wild steppe animals and livestock. The most common explanation for dzud points out that it develops as a result of prolonged droughts causing more frequent/widespread grassland fires thereby reducing the food base for animals and eventually leading to mass die-offs. The mortality of the animals becomes even higher when hot summers are followed by harsh and snowy winters because then the animals die of the effect of freeze superimposed on starvation (Fernández-Giménez et al., 2017). However, we hypothesize that the dzud can act as a trigger for extensive fires in the region. It happens when, due to dzud, large amounts of dry steppe plant biomass remain ungrazed, potentially serving as a fuel for the spring fires (Figs. 3, 7). Although, the hypothesis on a connection between natural fires and dzud seems promising, and is in line with the study by Karp et al. (2021) concluding on a link between enhanced fire activity throughout grassland ecosystems during the Quaternary and the extinction of large herbivores, definitely more research is required to document the long-term fire history records of Northern Mongolia. These studies can outline reference conditions to better understand the current and future relationships between human behaviors, climate, vegetation, permafrost, and fires (e.g., Dietze et al., 2018; Feurdean et al., 2020; Rudaya et al., 2020).

5. Conclusion

In this study, we investigated the interactions between the ecosystem and changing climatic conditions over the last 1000 years through changes in vegetation cover, sediment geochemistry, fires, and human activity, using the peat archive. Our results showed that within the last millennium the hydroclimatic conditions in the Khentii Mountains has changed substantially and the most pronounced changes occurred during the last century. We believe the changes observed in the fossil record are a regional reflection of human-induced global climatic warming. We also showed that during the Anthropocene, Mongolian steppes were prone to enhanced fires, the occurrence of which coincided with dzud, a deadly combination of summer droughts and snowy winters. The latter hypothesis seems very promising explanation of fire activity changes for the whole steppe zone. In broader sense, the study provides evidence that recent climate changes have already pushed parts of Northern Mongolia past the point where boreal forest mosaics are approaching its tipping point, which could lead to widespread shifts in fire regime and change forest to steppe biome. Because the study area is located in a patchy permafrost zone at the edge of the boreal forest, the ecosystems in this area are extremely sensitive to environmental factors, such as droughts and snowy winters (dzud occurring), which consequently make them more fire-prone. The Khentii Mountains as well as the entire northern area of Mongolia are dynamic ecosystems, with minimal land use, increasing hydroclimatic variability, and biodiversity stress. Therefore, in recent decades, the natural environment of Mongolia has been dynamically changing and its societies are living under continuous pressure of increasing heatwaves, intensifying fires, and permafrost degradation. All these factors strongly affect local economy.

Supplementary data to this article can be found online at https://doi.org/10.1016/j.scitotenv.2022.155660.

CRediT authorship contribution statement

MS conceived and designed the study, organized the expedition to Mongolia. MS and AS collected the core and conducted field measurements. ML and WSZ prepared the age-depth model. MS, MO, DŁ, AM and MW sampled the sediment core and performed the lab analysis. MS conducted the charcoal proxy analysis and MO conducted the pollen analysis. AK planned and performed statistical analyses. MS and co-authors wrote the paper, analyzed the data, prepared figures and/or tables, authored or reviewed drafts of the paper, and approved the final draft. All the authors reviewed the final manuscript.

Declaration of competing interest

The authors declare that they have no known competing financial interests or personal relationships that could have appeared to influence the work reported in this paper.

Acknowledgments

This research was funded and supported by grants from the National Science Centre, Poland (Grant no.: 2017/01/X/ST10/01216 and 2018/31/B/ST10/02498) and the program ***Polish-Mongolian Joint Research Project*** – "Environmental changes in the Northern Mongolia under recent and past climate variability". NR work was supported by the Russian Science Foundation (Grant No. 20-17-00110).

References

Andrews, L.O., Payne, R.J., Swindles, G.T., 2021. Testate amoebae as non-pollen palynomorphs in pollen slides: usefulness and application in palaeoenvironmental reconstruction. Applications of Non-Pollen Palynomorphs: from Palaeoenvironmental Reconstructions to Biostratigraphy. Geological Society of London, pp. 151–158.

van Asperen, E.N., Perrotti, A., Baker, A., 2021. Coprophilous fungal spores: non-pollen palynomorphs for the study of past megaherbivores. In: Applications of Non-Pollen Palynomorphs: from Palaeoenvironmental Reconstructions to Biostratigraphy. Geological Society of London 511, 245–267.

Bader, J., Jungclaus, J., Krivova, N., Lorenz, S., Maycock, A., Raddatz, T., et al., 2020. Global temperature modes shed light on the Holocene temperature conundrum. Nat. Commun. 11, 4726.

Bae, M.-J., Chon, T.-S., Park, Y.-S., 2014. Characterizing differential responses of benthic macroinvertebrate communities to floods and droughts in three different stream types using a self-organizing map. Ecohydrology 7, 115–126.

Beauregard, P., Lavoie, M., Pellerin, S., 2020. Recent gray birch (*Betula populifolia*) encroachment in temperate peatlands of eastern North America. Wetlands 40, 351–364.

Bedoya, D., Novotny, V., Manolakos, E.S., 2009. Instream and offstream environmental conditions and stream biotic integrity: importance of scale and site similarities for learning and prediction. Ecol. Model. 220, 2393–2406.

Berglund, B.E., Ralska-Jasiewiczowa, M., 1986. Pollen analysis. In: Berglund, B.E. (Ed.), Handbook of Holocene Palaeoecology and Palaeohydrology. John Wiley & Sons, Chichester, pp. 455–484.

Beug, H.-J., 2004. Leitfaden der Pollenbestimmung fur Mitteleuropa und angrenzende Gebiete. Pfeil, Munchen.

Birks, H.H., Birks, H.J.B., 1980. Quaternary Palaeoecology. Edward Arnold, London.

Biskaborn, B.K., Smith, S.L., Noetzli, J., Matthes, H., Vieira, G., Streletskiy, D.A., et al., 2019. Permafrost is warming at a global scale. Nat. Commun. 10, 264.

Boyle, J.F., 2001. Inorganic geochemical methods in palaeolimnology. In: Last, W., Smol, J. (Eds.), Tracking Environmental Change Using Lake Sediments. 2. Springer, Netherlands, pp. 83–141.

Bragazza, L., 2008. A climatic threshold triggers the die-off of peat mosses during an extreme heat wave. Glob. Change Biol. 14 (11), 2688–2695.

Bronk Ramsey, C., 2001. Development of the radiocarbon calibration program. Radiocarbon 43, 355–363.

Brosse, S., Giraudel, J.L., Lek, S., 2001. Utilisation of non-supervised neural networks and principal component analysis to study fish assemblages. Ecol. Model. 146, 159–166.

Bruel, R., Sabatier, P., 2020. Serac: an R package for ShortlivEd RAdionuclide chronology of recent sediment cores. J. Environ. Radioact. 225, 106449.

Charman, D.J., Beilman, D.W., Blaauw, M., Booth, R.K., Brewer, S., Chambers, F.M., et al., 2013. Climate-related changes in peatland carbon accumulation during the last millennium. Biogeosciences 10, 929–944.

Chen, F., Huang, X., Zhang, J., Holmes, J.A., Chen, J., 2006. Humid Little Ice Age in arid Central Asia documented by Bosten Lake, Xinjiang, China. Sci. China Ser. D Earth Sci. 49, 1280–1290.

Chen, F., Yu, Z., Yang, M., Ito, E., Wang, S., Madsen, D.B., et al., 2008. Holocene moisture evolution in arid Central Asia and its out-of-phase relationship with asian monsoon history. Quat. Sci. Rev. 27, 351–364.

Cheng, L., Lek, S., Lek-Ang, S., Li, Z., 2012. Predicting fish assemblages and diversity in shallow lakes in the Yangtze River basin. Limnologica 42, 127–136.

Churakova Sidorova, O.V., Corona, C., Fonti, M.V., Guillet, S., Saurer, M., Siegwolf, R.T.W., et al., 2020. Recent atmospheric drying in Siberia is not unprecedented over the last 1,500 years. Sci. Rep. 10, 15024.

Clark, J.S., 1988. Effect of climate change on fire regimes in northwestern Minnesota. Nature 334, 233–235.

Conedera, M., Tinner, W., Neff, C., Meurer, M., Dickens, A.F., Krebs, P., 2009. Reconstructing past fire regimes: methods, applications, and relevance to fire management and conservation. Quat. Sci. Rev. 28, 435–456.
Curtis, P.G., Slay, C.M., Harris, N.L., Tyukavina, A., Hansen, M.C., 2018. Classifying drivers of global forest loss. Science 361, 1108–1111.
Dagvadorj, D., Natsagdorj, L., Dorjpurev, J., Namkhainyam, B., 2009. Mongolia: Assessment Report on Climate Change. Ministry of Nature, Environment and Tourism, Ulaanbaatar, Mongolia.
Dangal, S.R.S., Tian, H., Lu, C., Pan, S., Pederson, N., Hessl, A., 2016. Synergistic effects of climate change and grazing on net primary production of Mongolian grasslands. Ecosphere 7 (5), e01274.
Dashtseren, A., Ishikawa, M., Iijima, Y., Jambaljav, Y., 2014. Temperature regimes of the active layer and seasonally frozen ground under a forest-steppe mosaic, Mongolia. Permafr. Periglac. Process. 25, 295–306.
Dashtseren, A., Temuujin, K., Westermann, S., Batbold, A., Amarbayasgalan, Y., Battogtokh, D., 2021. Spatial and temporal variations of freezing and thawing indices from 1960 to 2020 in Mongolia. Front. Earth Sci. 9, 713498.
Davi, N.K., D'Arrigo, R., Jacoby, G.C., Cook, E.R., Anchukaitis, K., Nachin, B., et al., 2015. A long-term context (931–2005 C.E.) for rapid warming over Central Asia. Quat. Sci. Rev. 121, 89–97.
Davis, M.B., Deevey Jr., E.S., 1964. Pollen accumulation rates: estimates from late-glacial sediment of Rogers Lake. Science 145, 1293–1295.
Dietze, E., Theuerkauf, M., Bloom, K., Brauer, A., Dörfler, W., Feeser, I., et al., 2018. Holocene fire activity during low-natural flammability periods reveals scale-dependent cultural human-fire relationships in Europe. Quat. Sci. Rev. 201, 44–56.
Dobricic, S., Russo, S., Pozzoli, L., Wilson, J., Vignati, E., 2020. Increasing occurrence of heat waves in the terrestrial Arctic. Environ. Res. Lett. 15 (2), 024022.
Dufrêne, M., Legendre, P., 1997. Species assemblages and indicator species: the need for a flexible asymmetrical approach. Ecol. Monogr. 67, 345–366.
Dugerdil, L., Joannin, S., Peyron, O., Jouffroy-Bapicot, I., Vannière, B., Boldgiv, B., et al., 2021. Climate reconstructions based on GDGT and pollen surface datasets from Mongolia and Baikal area: calibrations and applicability to extremely cold–dry environments over the Late Holocene. Clim. Past 17, 1199–1226.
Eimers, C.M., Dillon, P.J., Schiff, S.L., Jeffries, D.S., 2003. The effects of drying and re-wetting and increased temperature on sulphate release from upland and wetland material. Soil Biol. Biochem. 35, 1663–1673.
Enache, M.D., Cumming, B.F., 2006. Tracking recorded fires using charcoal morphology from the sedimentary sequence of Prosser Lake, British Columbia (Canada). Quat. Res. 65, 282–292.
Enache, M.D., Cumming, B.F., 2007. Charcoal morphotypes in lake sediments from British Columbia (Canada): an assessment of their utility for the reconstruction of past fire and precipitation. J. Paleolimnol. 38, 347–363.
Erdenebat, E., Sato, T., 2016. Recent increase in heat wave frequency around Mongolia: role of atmospheric forcing and possible influence of soil moisture deficit. Atmos. Sci. Lett. 17, 135–140.
Etzelmüller, B., Heggem, E.S.F., Sharkhuu, N., Frauenfelder, R., Kääb, A., Goulden, C., 2006. Mountain permafrost distribution modelling using a multi-criteria approach in the Hövsgöl area, northern Mongolia. Permafr. Periglac. Process. 17, 91–104.
Faegri, K., Iversen, J., Kaland, P.E., Krzywinski, K., 2000. Textbook of Pollen Analysis. Blackburn Press.
Falk, D.A., Watts, A.C., Thode, A.E., 2019. Scaling ecological resilience. Front. Ecol. Evol. 7, 275.
Fernández-Giménez, M.E., Venable, N.H., Angerer, J., Fassnacht, S.R., Reid, R.S., Khishigbayar, J., 2017. Exploring linked ecological and cultural tipping points in Mongolia. Anthropocene 17, 46–69.
Feurdean, A., Vannière, B., Finsinger, W., Warren, D., Connor, S.C., Forrest, M., et al., 2020. Fire hazard modulation by long-term dynamics in land cover and dominant forest type in Eastern and Central Europe. Biogeosciences 17, 1213–1230.
van Geel, B., Aptroot, A., 2006. Fossil ascomycetes in Quaternary deposits. Nova Hedwigia 82, 313–329.
Fiałkiewicz-Kozieł, B., Smieja-Król, B., Frontasyeva, M., Słowiński, M., Marcisz, K., Lapshina, E., et al., 2016. Anthropogenic- and natural sources of dust in peatland during the Anthropocene. Sci. Rep. 6, 38731.
Ghazoul, J., Burivalova, Z., Garcia-Ulloa, J., King, L.A., 2015. Conceptualizing forest degradation. Trends Ecol. Evol. 30, 622–632.
Graham, E.B., Averill, C., Bond-Lamberty, B., Knelman, J.E., Krause, S., Peralta, A.L., et al., 2021. Toward a generalizable framework of disturbance ecology through crowdsourced science. Front. Ecol. Evol. 9, 588940. https://doi.org/10.3389/fevo.2021.588940.
Grimm, E.C., 1991. Tilia and Tilia Graph: llinois State Museum.
Gunin, P.D., Vostokova, E.A., Dorofeyuk, N.I., Tarasov, P.E., Black, C.C., 1999. Vegetation Dynamics of Mongolia. Springer, Dordrecht.
Hahn, A., Kliem, P., Ohlendorf, C., Zolitschka, B., Rosén, P., 2013. Climate induced changes as registered in inorganic and organic sediment components from Laguna Potrok Aike (Argentina) during the past 51 ka. Quat. Sci. Rev. 71, 154–166.
Halsall, K.M., Ellingsen, V.M., Asplund, J., Bradshaw, R.H.W., Ohlson, M., 2018. Fossil charcoal quantification using manual and image analysis approaches. The Holocene 28 (8), 1345–1353.
Hammer, Ø., Harper, D.A.T., Ryan, P.D., 2001. PAST: paleontological statistics software package for education and data analysis. Palaeontol. Electron. 4.
Harris, C., Arenson, L.U., Christiansen, H.H., Etzelmüller, B., Frauenfelder, R., Gruber, S., et al., 2009. Permafrost and climate in Europe: monitoring and modelling thermal, geomorphological and geotechnical responses. Earth Sci. Rev. 92, 117–171.
Hawthorne, D., Courtney Mustaphi, C.J., Aleman, J.C., Blarquez, O., Colombaroli, D., Daniau, A.-L., et al., 2018. Global modern charcoal dataset (GMCD): a tool for exploring proxy-fire linkages and spatial patterns of biomass burning. Quat. Int. 488, 3–17.
Hessl, A.E., Brown, P., Byambasuren, O., Cockrell, S., Leland, C., Cook, E., et al., 2016. Fire and climate in Mongolia (1532–2010 Common Era). Geophys. Res. Lett. 43, 6519–6527.
Hessl, A.E., Anchukaitis, K.J., Jelsema, C., Cook, B., Byambasuren, O., Leland, C., et al., 2018. Past and future drought in Mongolia. Sci. Adv. 4, e170183.
Hinzke, T., Li, G., Tanneberger, F., Seeber, E., Aggenbach, C., Lange, J., et al., 2021. Potentially peat-forming biomass of fen sedges increases with increasing nutrient levels. Funct. Ecol. 35, 1579–1595.
Hiyama, T., Dashtseren, A., Asai, K., Kanamori, H., Iijima, Y., Ishikawa, M., 2021. Groundwater age of spring discharges under changing permafrost conditions: the Khangai Mountains in Central Mongolia. Environ. Res. Lett. 16, 015008.
IPCC, 2018. In: Masson-Delmotte, V., Zhai, P., Pörtner, H.-O., Roberts, D., Skea, J., Shukla, P.R. (Eds.), Global Warming of 1.5°C. An IPCC Special Report on the Impacts of Global Warming of 1.5°C Above Pre-industrial Levels and Related Global Greenhouse Gas Emission Pathways, in the Context of Strengthening the Global Response to the Threat of Climate Change, Sustainable Development, and Efforts to Eradicate Poverty.
Ishikawa, M., Jamvaljav, Y., Dashtseren, A., Sharkhuu, N., Davaa, G., Iijima, Y., et al., 2018. Thermal states, responsiveness and degradation of marginal permafrost in Mongolia. Permafr. Periglac. Process. 29, 271–282.
Jankovská, V., Komárek, J., 2000. Indicative value of *Pediastrum* and other coccal green algae in palaeoecology. Folia Geobot. 35, 59–82.
Karp, A.T., Faith, J.T., Marlon, J.R., Staver, A.C., 2021. Global response of fire activity to late Quaternary grazer extinctions. Science 374, 1145–1148.
Kelly, L.T., Giljohann, K.M., Duane, A., Aquilue, N., Archibald, S., Batllori, E., et al., 2020. Fire and biodiversity in the Anthropocene. Science 370, eabb0355.
Kharuk, V.I., Ponomarev, E.I., Ivanova, G.A., Dvinskaya, M.L., Coogan, S.C.P., Flannigan, M.D., 2021. Wildfires in the Siberian taiga. Ambio 50, 1953–1974.
Klinge, M., Dulamsuren, C., Erasmi, S., Karger, D.N., Hauck, M., 2018. Climate effects on vegetation vitality at the treeline of boreal forests of Mongolia. Biogeosciences 15, 1319–1333.
Klinge, M., Dulamsuren, C., Schneider, F., Erasmi, S., Bayarsaikhan, U., Sauer, D., et al., 2021a. Geoecological parameters indicate discrepancies between potential and actual forest area in the forest-steppe of Central Mongolia. For. Ecosyst. 8, 55.
Klinge, M., Schneider, F., Dulamsuren, C., Arndt, K., Bayarsaikhan, U., Sauer, D., 2021b. Interrelations between relief, vegetation, disturbances, and permafrost in the forest-steppe of Central Mongolia. Earth Surf. Process. Landf. 46, 1766–1782.
Kohonen, T., 1982. Self-organized formation of topologically correct feature maps. Biol. Cybern. 43, 59–69.
Kohonen, T., 2001. Self-Organizing Maps. Springer, Berlin.
Komárek, J., Marvan, P., 1992. Morphological differences in natural populations of the genus *Botryococcus* (Chlorophyceae). Arch. Protistenkd. 141, 65–100.
Kopp, B.J., Lange, J., Menzel, L., 2017. Effects of wildfire on runoff generating processes in northern Mongolia. Reg. Environ. Change 17, 1951–1963.
Koretsky, C.M., Haas, J.R., Ndenga, N.T., Miller, D., 2006. Seasonal variations in vertical redox stratification and potential influence on trace metal speciation in minerotrophic peat sediments. Water Air Soil Pollut. 173, 373–403.
Kuuluvainen, T., Gauthier, S., 2018. Young and old forest in the boreal: critical stages of ecosystem dynamics and management under global change. For. Ecosyst. 5, 26.
Lan, J., Xu, H., Sheng, E., Yu, K., Wu, H., Zhou, K., et al., 2018. Climate changes reconstructed from a glacial lake in High Central Asia over the past two millennia. Quat. Int. 487, 43–53.
Lange, J., Kopp, B.J., Bents, M., Menzel, L., 2015. Tracing variability of run-off generation in mountainous permafrost of semi-arid North-Eastern Mongolia. Hydrol. Process. 29, 1046–1055.
Lasne, E., Lek, S., Laffaille, P., 2007. Patterns in fish assemblages in the Loire floodplain: the role of hydrological connectivity and implications for conservation. Biol. Conserv. 139, 258–268.
Lehmkuhl, F., Hilgers, A., Fries, S., Hülle, D., Schlütz, F., Shumilovskikh, L., et al., 2011. Holocene geomorphological processes and soil development as indicator for environmental change around Karakorum, upper Orkhon Valley (Central Mongolia). Catena 87, 31–44.
Lek, S., Guégan, J.F., 1999. Artificial neural networks as a tool in ecological modelling, an introduction. Ecol. Model. 120, 65–73.
Lek, S., Scardi, M., Verdonschot, P.F.M., Descy, J.P., Park, Y.S. (Eds.), 2005. Modelling Community Structure in Freshwater Ecosystems. Springer, Berlin.
Lenton, T.M., Rockstrom, J., Gaffney, O., Rahmstorf, S., Richardson, K., Steffen, W., et al., 2019. Climate tipping points – too risky to bet against. Nature 575, 592–595.
Li, Y., Vitt, D.H., 2013. The dynamics of moss establishment: temporal responses to a moisture gradient. J. Bryol. 18, 677–687.
Loisel, J., Yu, Z., Beilman, D.W., Camill, P., Alm, J., Amesbury, M.J., et al., 2014. A database and synthesis of northern peatland soil properties and Holocene carbon and nitrogen accumulation. The Holocene 24, 1028–1042.
Long, T., Zhang, Z., He, G., Jiao, W., Tang, C., Wu, B., et al., 2019. 30 m resolution global annual burned area mapping based on Landsat images and Google Earth Engine. Remote Sens. 11, 489.
Mackay, J.R., 1998. Pingo growth and collapse, Tuktoyaktuk peninsula area, Western Arctic coast, Canada: a long-term field study. Géog. Phys. Quatern. 52, 1–53.
Mandel, W., 1949. Outer Mongolia's five-year plan. Far Eastern Surv. 18, 140–144.
Mefford, M.J., McCune, B., 2011. PC-ORD. Multivariate analysis of Ecological Data Version 6.0 for Windows. p. 28.
Minderlein, S., Menzel, L., 2015. Evapotranspiration and energy balance dynamics of a semi-arid mountainous steppe and shrubland site in northern Mongolia. Environ. Earth Sci. 73, 593–609.
Miner, K.R., Turetsky, M.R., Malina, E., Bartsch, A., Tamminen, J., McGuire, A.D., et al., 2022. Permafrost carbon emissions in a changing Arctic. Nat. Rev. Earth Environ. 3, 55–67.
Mooney, S.D., Tinner, W., 2010. The analysis of charcoal in peat and organic sediments. Mires Peat 7, 1–18.
Moore, P.D., Webb, J.A., Collinson, M.E., 1991. Pollen Analysis. Blackwell, Oxford.
Mustaphi, C.J.C., Pisaric, M.F.J., 2014. A classification for macroscopic charcoal morphologies found in Holocene lacustrine sediments. Prog. Phys. Geogr. Earth Environ. 38, 734–754.

Ney, J.J., 1993. Practical use of biological statistics. In: Kohler C.C., Hubert W.A. (Eds.), Inland Fisheries Management of North America. American Fisheries Society, Bethesda, pp. 137–158.

Obu, J., Westermann, S., Bartsch, A., Berdnikov, N., Christiansen, H.H., Dashtseren, A., et al., 2019. Northern Hemisphere permafrost map based on TTOP modelling for 2000–2016 at 1 km^2 scale. Earth Sci. Rev. 193, 299–316.

Park, Y.-S., Kwon, Y.-S., Hwang, S.-J., Park, S., 2014. Characterizing effects of landscape and morphometric factors on water quality of reservoirs using a self-organizing map. Environ. Model. Softw. 55, 214–221.

Payne, A.E., Demory, M.-E., Leung, L.R., Ramos, A.M., Shields, C.A., Rutz, J.J., et al., 2020. Responses and impacts of atmospheric rivers to climate change. Nat. Rev. Earth Environ. 1 (3), 143–157.

Pendergrass, A.G., Meehl, G.A., Pulwarty, R., Hobbins, M., Hoell, A., AghaKouchak, A., et al., 2020. Flash droughts present a new challenge for subseasonal-to-seasonal prediction. Nat. Clim. Change 10, 191–199.

Perkins-Kirkpatrick, S.E., Lewis, S.C., 2020. Increasing trends in regional heatwaves. Nat. Commun. 11, 3357.

Płóciennik, M., Kruk, A., Michczyńska, D.J., Birks, J.B., 2015. Kohonen artificial neural networks and the IndVal index as supplementary tools for the quantitative analysis of palaeoecological data. Geochronometria 42, 189–201.

Punsalmaa, B., 2006. Climate Change Vulnerability and Adaptation in the Livestock Sector of Mongolia. Institute of Meteorology and Hydrology, Ulaanbaatar, Mongolia, The International START Secretariat 2000 Florida Avenue, NW Washington, DC 20009 USA, pp. 84.

Putnam, A.E., Putnam, D.E., Andreu-Hayles, L., Cook, E.R., Palmer, J.G., Clark, E.H., et al., 2016. Little Ice Age wetting of interior Asian deserts and the rise of the Mongol Empire. Quat. Sci. Rev. 131, 33–50.

Quinn, G.P., Keough, M.J., 2002. Experimental Design and Data Analysis for Biologists. Cambridge University Press.

Reyer, C.P.O., Brouwers, N., Rammig, A., Brook, B.W., Epila, J., Grant, R.F., et al., 2015. Forest resilience and tipping points at different spatio-temporal scales: approaches and challenges. J. Ecol. 103, 5–15.

Rudaya, N., Krivonogov, S., Słowiński, M., Cao, X., Zhilich, S., 2020. Postglacial history of the steppe Altai: climate, fire and plant diversity. Quat. Sci. Rev. 249, 106616.

Schlütz, F., Dulamsuren, C., Wieckowska, M., Mühlenberg, M., Hauck, M., 2008. Late Holocene vegetation history suggests natural origin of steppes in the northern Mongolian mountain taiga. Palaeogeogr. Palaeoclimatol. Palaeoecol. 261, 203–217.

Schneider, F., Klinge, M., Brodthuhn, J., Peplau, T., Sauer, D., 2021. Hydrological soil properties control tree regrowth after forest disturbance in the forest steppe of Central Mongolia. Soil 7, 563–584.

Schoennagel, T., Balch, J.K., Brenkert-Smith, H., Dennison, P.E., Harvey, B.J., Krawchuk, M.A., et al., 2017. Adapt to more wildfire in western North American forests as climate changes. Proc. Natl. Acad. Sci. U. S. A. 114, 4582–4590.

Shumilovskikh, L., O'Keefe, J.M.K., Marret, F., 2021. An overview of the taxonomic groups of non-pollen palynomorphs. Geol. Soc. Lond., Spec. Publ. 511, 13–61.

Słowiński, M., Marcisz, K., Płóciennik, M., Obremska, M., Pawłowski, D., Okupny, D., et al., 2016. Drought as a stress driver of ecological changes in peatland – a palaeoecological study of peatland development between 3500 BCE and 200 BCE in central Poland. Palaeogeogr. Palaeoclimatol. Palaeoecol. 461, 272–291.

Słowiński, M., Skubała, P., Zawiska, I., Kruk, A., Obremska, M., Milecka, K., et al., 2018. Cascading effects between climate, vegetation, and macroinvertebrate fauna in 14,000-year palaeoecological investigations of a shallow lake in eastern Poland. Ecol. Indic. 85, 329–341.

Stivrins, N., Aakala, T., Ilvonen, L., Pasanen, L., Kuuluvainen, T., Vasander, H., et al., 2019. Integrating fire-scar, charcoal and fungal spore data to study fire events in the boreal forest of northern Europe. The Holocene 29, 1480–1490.

Stockmarr, J., 1971. Tablets with spores used in absolute pollen analysis. Pollen Spores 13, 615–621.

Szajdak, L.W., Jezierski, A., Wegner, K., Meysner, T., Szczepański, M., 2020. Influence of drainage on peat organic matter: implications for development, stability, and transformation. Molecules 25, 2587.

Tian, F., Herzschuh, U., Mischke, S., Schlütz, F., 2014. What drives the recent intensified vegetation degradation in Mongolia – climate change or human activity? The Holocene 24, 1206–1215.

Tian, F., Cao, X., Dallmeyer, A., Lohmann, G., Zhang, X., Ni, J., et al., 2017. Biome changes and their inferred climatic drivers in northern and eastern continental Asia at selected times since 40 cal ka BP. Veg. Hist. Archaeobotany 27 (2), 365–379.

Turetsky, M.R., Abbott, B.W., Jones, M.C., Anthony, K.W., Olefeldt, D., Schuur, E.A.G., et al., 2019. Permafrost collapse is accelerating carbon release. Nature 569, 32–34.

Turetsky, M.R., Abbott, B.W., Jones, M.C., Anthony, K.W., Olefeldt, D., Schuur, E.A.G., et al., 2020. Carbon release through abrupt permafrost thaw. Nat. Geosci. 13, 138–143.

Umbanhowar, C.E., Shinneman, A.L.C., Tserenkhand, G., Hammon, E.R., Lor, P., Nail, K., 2009. Regional fire history based on charcoal analysis of sediments from nine lakes in western Mongolia. The Holocene 19, 611–624.

Unkelbach, J., Kashima, K., Enters, D., Dulamsuren, C., Punsalpaamuu, G., Behling, H., 2019. Late Holocene (Meghalayan) palaeoenvironmental evolution inferred from multi-proxy-studies of lacustrine sediments from the Dayan Nuur region of Mongolia. Palaeogeogr. Palaeoclimatol. Palaeoecol. 530, 1–14.

Van Loon, A.F., Gleeson, T., Clark, J., Van Dijk, A.I.J.M., Stahl, K., Hannaford, J., et al., 2016. Drought in the Anthropocene. Nat. Geosci. 9, 89–91.

Vannière, B., Colombaroli, D., Chapron, E., Leroux, A., Tinner, W., Magny, M., 2008. Climate versus human-driven fire regimes in Mediterranean landscapes: the Holocene record of Lago dell'Accesa (Tuscany, Italy). Quat. Sci. Rev. 27, 1181–1196.

Vesanto, J., Alhoniemi, E., 2000. Clustering of the self-organizing map. IEEE Trans. Neural Netw. 11, 586–600.

Vesanto, J., Himberg, J., Alhoniemi, E., Parhankangas, J., 2000. SOM Toolbox for Matlab 5.

Walsh, M.K., Lukens, M.L., McCutcheon, P.T., Burtchard, G.C., 2017. Fire-climate-human interactions during the postglacial period at Sunrise Ridge, Mount Rainier National Park, Washington (USA). Quat. Sci. Rev. 177, 246–264.

Walsh, M.K., Duke, H.J., Haydon, K.C., 2018. Toward a better understanding of climate and human impacts on late Holocene fire regimes in the Pacific Northwest, USA. Prog. Phys. Geogr. Earth Environ. 42, 478–512.

Ward, J.H., 1963. Hierarchical grouping to optimize an objective function. J. Am. Stat. Assoc. 58, 236–244.

Warner, B.G., Chengalath, R., 1988. Holocene fossil *Habrotrocha angusticollis* (Bdelloidea: Rotifera) in North America. J. Paleolimnol. 1.

Whitlock, C., Larsen, C., 2001. Charcoal as a fire proxy. In: Smol, J.P., HJB, Birks, Last, W.M. (Eds.), Tracking Environmental Change Using Lake Sediments. Volume 3: Terrestrial, Algal, and Siliceous Indicators. Springer, Netherlands, pp. 75–97.

Yao, Y., Lan, J., Zhao, J., Vachula, R.S., Xu, H., Cai, Y., et al., 2020. Abrupt freshening since the early Little Ice Age in Lake Sayram of arid Central Asia inferred from an alkenone isomer proxy. Geophys. Res. Lett. 47, e2020GL089257.

Żarczyński, M., Wacnik, A., Tylmann, W., 2019. Tracing lake mixing and oxygenation regime using the Fe/Mn ratio in varved sediments: 2000 year-long record of human-induced changes from Lake Żabińskie (NE Poland). Sci. Total Environ. 657, 585–596.

Zarzycki, K., Trzcińska-Tacik, H., Różański, W., Szeląg, Z., Wołek, J., Korzeniak, U., 2002. Ecological indicator values of vascular plants of Poland. W. Szafer Institute of Botany Polish Academy of Sciences, Kraków, pp. 183.

Zhang, Q., Zhang, J., Suriguga, Zhang, B., Cheng, J., Tian, S., 2011. Self-organizing feature map classification and ordination of *Larix principis-rupprechtii* forest in Pangquangou Nature Reserve. Acta Ecol. Sin. 31, 2990–2998.

Zibulski, R., Wesener, F., Wilkes, H., Plessen, B., Pestryakova, L.A., Herzschuh, U., 2017. C/N ratio, stable isotope ($\delta^{13}C$, $\delta^{15}N$), and *n*-alkane patterns of brown mosses along hydrological gradients of low-centred polygons of the Siberian Arctic. Biogeosciences 14, 1617–1630.